arXiv:2405.19405v2 [cond-mat.mes-hall] 25 Oct 2024

Quarter- and half-filled quantum Hall states and their competing interactions in bilayer graphene

Ravi Kumar[1,*], André Haug[1,*], Jehyun Kim[1], Misha Yutushui[1], Konstantin Khudiakov[1], Vishal Bhardwaj[1], Alexey Ilin[1], K. Watanabe[2], T. Taniguchi[3], David F. Mross[1], and Yuval Ronen[1†]

[1]*Department of Condensed Matter Physics, Weizmann Institute of Science, Rehovot 76100, Israel.*
[2]*Research Center for Functional Materials, National Institute for Materials Science, 1-1 Namiki, Tsukuba 305-0044, Japan.*
[3]*International Center for Materials Nanoarchitectonics, National Institute for Materials Science, 1-1 Namiki, Tsukuba 305-0044, Japan.*

Bilayer graphene has emerged as a key platform for non-Abelian fractional quantum Hall (FQH) states, exhibiting multiple half-filled plateaus with large energy gaps. Here, we report four unexpected quarter-filled states and complete the sequence of half-filled plateaus by observing the previously missing $\nu = -\frac{3}{2}$ and $\nu = \frac{1}{2}$ states. Identifying the half-filled plateaus according to their Levin–Halperin daughter states, we reveal an alternating pattern of non-Abelian topological orders. Whenever a pair of $N = 1$ Landau levels cross, anti-Pfaffian and Pfaffian develop in the lower and higher levels, respectively. Surprisingly, quarter states occur in $N = 0$ levels and are also accompanied by daughters. The mutual exclusion of half- and quarter-filled states indicates a robust competition between the interactions favoring paired states of either two-flux or four-flux composite fermions. Finally, we observe several FQH states that require strong interactions between composite fermions. The systematic pattern of non-Abelian states across two generations of even denominators strengthens the identification of their topological orders and suggests a universal origin.

Introduction. The search for non-Abelian anyons has inspired groundbreaking research into the nature of the even-denominator fractional quantum Hall (FQH) states.[1] However, decades after the initial observation of a plateau at filling factor $\nu = \frac{5}{2}$ in GaAs,[2] its nature and origin remain under intense debate.[3] This enduring mystery stems from a rich competition between multiple exotic quantum states, which includes several sought-after non-Abelian states[4–8] contending with more conventional Abelian states[1,9] and metallic composite-fermion liquids.[10] Recent observations of plateaus at half filling in different semiconductor devices[11–16] and van der Waals materials[17–23] hint at diverse non-Abelian phases whose origins are yet to be unveiled.

Composite fermions (CFs), electrons bound to a pair of flux quanta and carrying a charge of $q_{\mathrm{CF}} = (1-2\nu)e$, are pivotal for explaining half-filled states.[24] At half filling, CFs are charge neutral and impervious

*These authors contributed equally: Ravi Kumar, André Haug
†yuval.ronen@weizmann.ac.il

to magnetic fields. Consequently, they can form a metallic Fermi surface,[10] which is commonly observed in the half-filled zeroth Landau level (0LL). At the same filling, incompressible states develop when the metallic state transitions into a CF superconductor. The attraction necessary for CF pairing arises in the first excited Landau level (1LL), whose single-electron in-plane wave functions differ from those of the 0LL.[25] Alternatively, pairing can be promoted in wide quantum wells where wave functions extend out-of-plane.[26,27] However, the choice of the pairing channel—and thus, whether the state exhibits Abelian or non-Abelian characteristics—is influenced by subtle effects such as Landau-level mixing. Even more elusive are states formed at quarter fillings, previously reported in GaAs[28–32] and monolayer graphene.[33] These states comprise charge-neutral pairs of four-flux composite fermions, ^{4}CFs, which condense into a superfluid, similar to the case at half filling.[34,35]

Attractive interactions at half filling are detrimental to FQH states of the Jain sequence $\nu = \frac{n}{2n+1}$. At these fillings, the CF charge q_{CF} is non-zero. Consequently, these CFs are sensitive to magnetic fields, and the CF metal exhibits Shubnikov–de Haas (SdH) oscillations, which manifest as incompressible Jain states.[36] When a pairing gap forms on the composite Fermi surface, the SdH oscillations are suppressed, and even lower-order Jain states vanish around half-filled plateaus.[2] A compromise between pairing and adjusting to the magnetic field takes the form of 'daughter' states, first proposed by Levin and Halperin.[37] In these states, paired CFs enter bosonic quantum Hall states instead of condensing, resulting in FQH states at distinct filling factors determined by the pairing channel.[38,39] The unique parent–daughter correspondence enables the identification of topological orders at half filling through straightforward bulk transport measurements.

Bilayer graphene (BLG) has established itself as a versatile platform for studying the superconductivity of both electrons[40] and CFs in even-denominator states.[17–19,22] An important feature is the possibility of tuning the Landau level spectrum, spanned by spin, valley, and orbital quantum numbers[41] (see Fig. 1A) and split by interactions,[18,42,43] through independently controlling filling factor and displacement field. By exploring this phase space, plateaus at multiple distinct half-integer fillings have been identified according to their daughter states[22,23,44]. However, the periodic pattern of non-Abelian states remained hidden due to missing plateaus $\nu = -\frac{3}{2}$ and $\nu = \frac{1}{2}$. Quantum Hall states at quarter-integer fillings and other 'next-generation'[32,45,46] even denominators had not been seen in BLG.

In this work, we report the observation of incompressible FQH states at quarter- and half-filled Landau levels in BLG. First, our measurement of additional plateaus at $\nu = -\frac{3}{2}$ and $\nu = \frac{1}{2}$ reaffirms an orbital index of $N = 1$ as a prerequisite to forming incompressible states at half fillings. By observing their daughters, we identify both states as anti-Pfaffian. These plateaus complete the sequence of previously known states and reveal a systematic alternation between anti-Pfaffian and Pfaffian in odd and even Landau levels, respectively. Second, we observe the emergence of incompressible states at four distinct quarter-integer fillings. Surprisingly, all these plateaus arise in $N = 0$ levels, which are not expected to favor

CF pairing.[47] The topological order of three among the newly discovered quarter states is constrained to the non-Abelian anti-Pfaffian or Abelian anti-(331) by clearly resolved daughter states. The formation of quarter-filled states only at $N = 0$, in contrast to half-filled states only at $N = 1$, indicates a robust competition between the interactions favoring either paired states of ^{4}CFs or of ^{2}CFs, respectively. Finally, we observed odd and even 'next-generation' FQH states at partial fillings of ^{2}CFs.

Results. Our devices (device 1 and device 2) consist of BLG encapsulated by hexagonal boron nitride and graphite layers acting as gates;[48] see Materials and Methods section. Subsequently, we fabricated the heterostructures into a Hall bar, as shown in Supplementary Material (SM) Sec. 1. The electrical transport properties of device 1 were measured in a dilution refrigerator with a base temperature $T = 16$ mK and a magnetic field B up to 18 T. Device 2 was measured in another dilution refrigerator with a base temperature $T = 10$ mK and a magnetic field up to 12 T. The data shown in the main manuscript are from device 1 and are consistent with those of device 2 (see SM Sec. 12). Using a standard low-frequency lock-in technique, we measured the longitudinal (R_{xx}) and transverse (R_{xy}) resistances; see SM Sec. 1. The dual-gate geometry permits independent tuning of filling factor ν and displacement field D, thus granting control over both the orbital ($N = 0, 1$) and the valley isospin (K, K').[18,42]

Fig. 1B shows R_{xx} and R_{xy} as a function of ν at $D = -80$ mV/nm and $B = 18$ T, where the integer LL has an $N = 0$ orbital. We observe a compressible ^{2}CF metal at $\nu = \frac{1}{2}$, flanked by an abundance of SdH oscillations, testifying to the low disorder of the device. As we increase the displacement field to $D = -160$ mV/nm, the Landau level transitions to $N = 1$. Here, we observe an incompressible state at $\nu = \frac{1}{2}$ and a strong suppression of the Jain states; see Fig. 1C. The diminished R_{xx} along with a quantized plateau in R_{xy} indicates pairing of ^{2}CFs at $\nu = \frac{1}{2}$. Surprisingly, near $\nu = \frac{3}{4}$, the roles of $N = 0$ and $N = 1$ are reversed: For $N = 0$, we observe a strong suppression of R_{xx} along with a plateau in R_{xy} at $\nu = \frac{3}{4}$, indicating the pairing of ^{4}CFs. By contrast, at $N = 1$, this filling hosts a compressible ^{4}CF metal flanked by SdH oscillations. Fig. 1D shows an extended measurement over a continuous range of D which confirms the robustness of both half- and quarter-filled states. Moreover, it shows that these states form irrespective of the valley isospin. Notice that the position of the FQH states changes slightly as either D or B are varied, consistent with previous works.[18,22] We attribute this effect to a change in quantum capacitance. Subsequently, FQH states were labelled according to their R_{xy} values and the position of their R_{xx} minima with respect to other states. The quarter- and half-filled states at $\nu = \frac{3}{4}$ and $\nu = \frac{1}{2}$ were also observed in device 2, see SM Sec 12.

We observed all previously reported half-filled states at $\nu = -\frac{5}{2}, -\frac{1}{2}, \frac{3}{2}, \frac{5}{2}, \frac{7}{2}$ along with the same daughter states[22]. The new half-filled state at $\nu = -\frac{3}{2}$ emerges in a single pocket around $D = 0$, accompanied by daughter states $\nu = -\frac{20}{13}, -\frac{25}{17}$. The one at $\nu = \frac{1}{2}$ occurs in two pockets with opposite D polarity, with daughters at $\nu = \frac{6}{13}, \frac{9}{17}$. All half-filled states develop only at $N = 1$, where the Jain states are strongly suppressed, and quarter-filled states are absent.

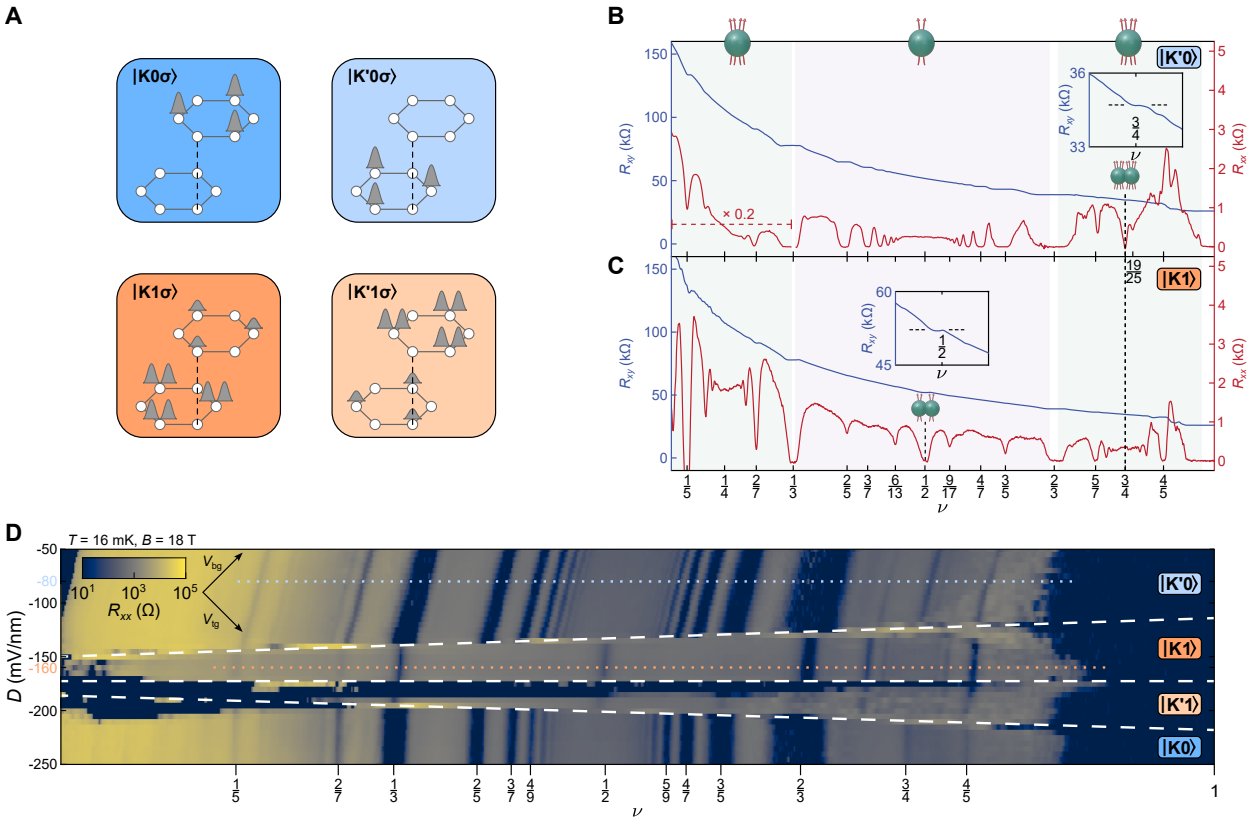


Figure 1: Interplay between quarter- and half-filled FQH states in BLG. (**A**) BLG unit cell's real space single-electron wave functions for the 0LL, eightfold degenerate in valley isospin, orbital, and spin. (**B**,**C**) Longitudinal R_{xx} (red) and transverse R_{xy} (blue) resistances as a function of ν at $T = 16$ mK, $B = 18$ T for $D = -80$ mV/nm ($N = 0$) (B) and $D = -160$ mV/nm ($N = 1$) (C). Panels in the top right corners indicate the valley isospin and orbital. The shaded purple (center) and green (sides) regions correspond to FQH states composed of ^{2}CFs and ^{4}CFs. The insets show zoom-ins to R_{xy} plateaus at $\nu = \frac{1}{2}$ (C) and $\nu = \frac{3}{4}$ (B). We attribute these plateaus to pairing of ^{2}CFs and ^{4}CFs, respectively. In (B), R_{xx} data below $\nu = \frac{1}{3}$ were divided by 5 to accommodate large R_{xx} values. (**D**) R_{xx} as a function of ν and D, controlled electrostatically by altering the back and top gate voltages, $V_{\rm bg}$ and $V_{\rm tg}$. The dotted horizontal lines at $D = -80$ mV/nm (light blue) and $D = -160$ mV/nm (orange) indicate the line cuts displayed in (B) and (C), respectively.

To look for additional quarter-filled states, we broaden our study to all eight levels comprising the 0LL. In Fig. 2A, we show R_{xx} as a function of ν and D for the hole-doped (left) and electron-doped (right) sides. Dark-blue areas mark $R_{xx} < 10\ \Omega$ where the bulk becomes incompressible. On the hole (electron) side, the R_{xx} measurement is overshadowed by artifacts for negative (positive) D due to the contact's fabrication scheme; see Materials and Methods section.

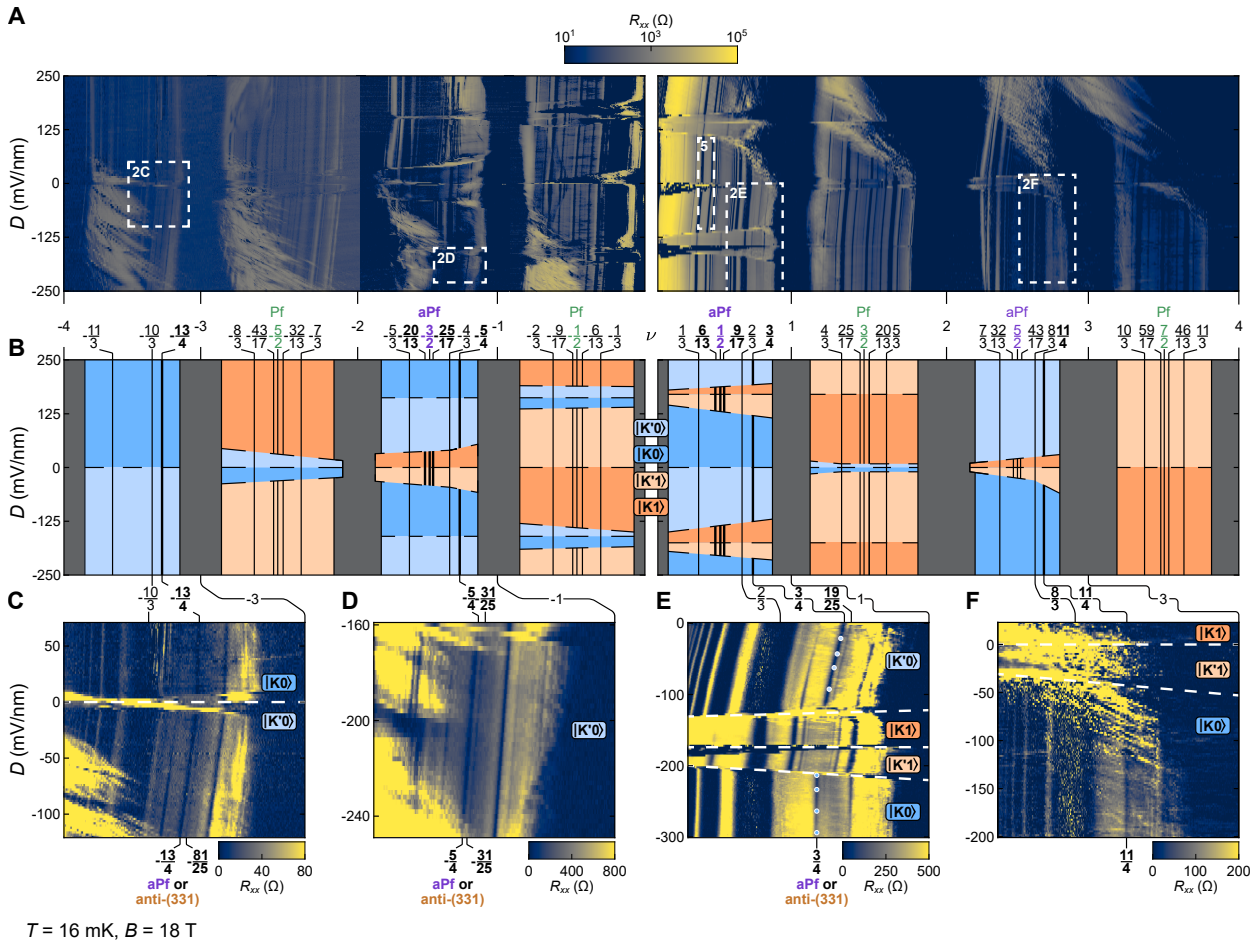


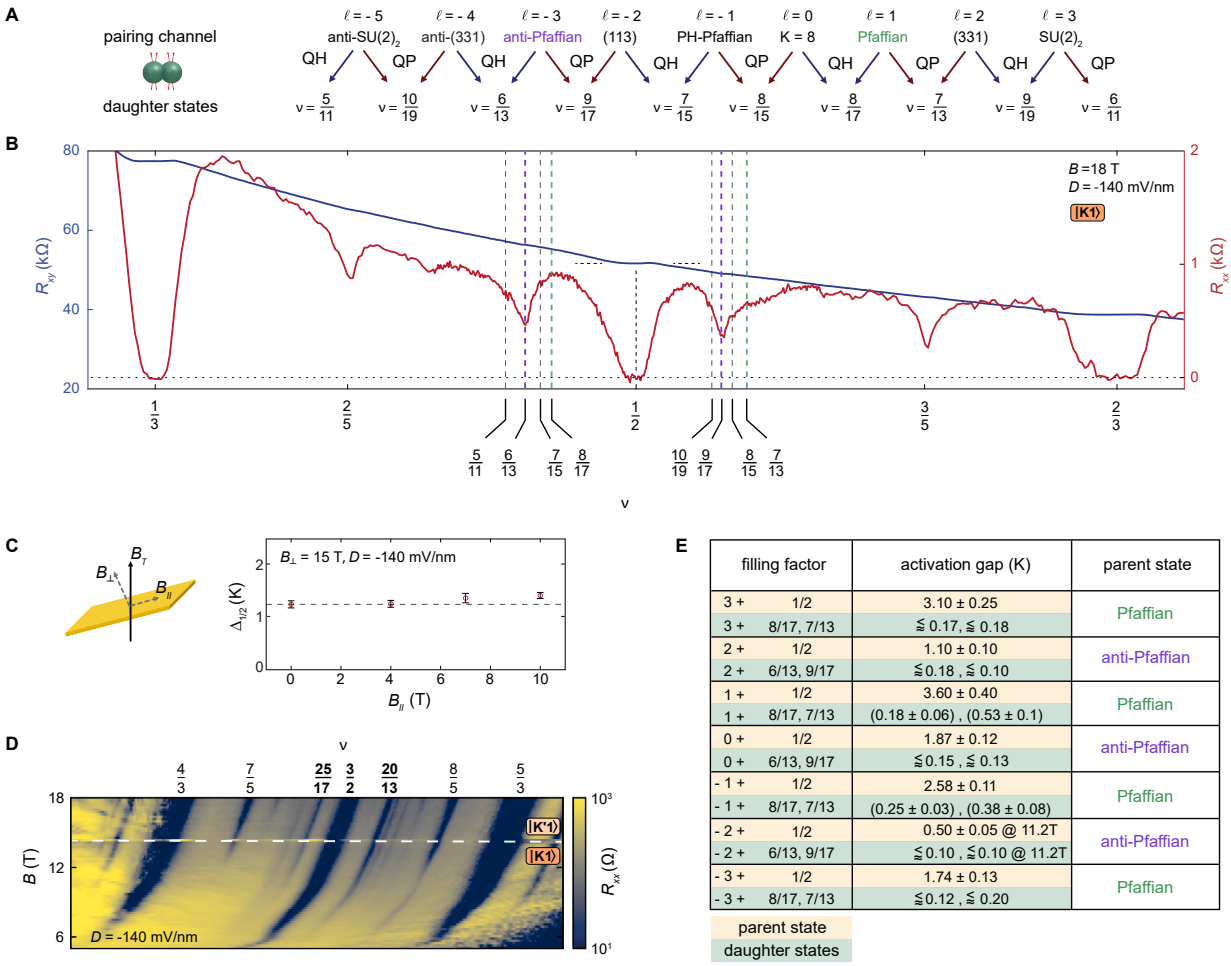
Figure 2: Even-denominator FQH states in the 0LL of BLG. (**A**) R_{xx} as a function of ν and D for $-4 \leq \nu < 0$ (left panel) and $0 < \nu \leq 4$ (right panel). Areas highlighted by dashed white lines refer to high-resolution measurements in (C-F) and Fig. 5. See SM Sec. 4 for enlarged view. (**B**) Schematic summary of all even- and selected odd-denominator FQH states observed in (A), with higher-order Jain states omitted to increase visibility. Vertical lines mark observed FQH states; bold vertical lines mark newly observed FQH states. Dashed lines mark valley and orbital crossings along the (ν, D) phase space. Green and purple labels indicate Pfaffian (Pf) and anti-Pfaffian (aPf) states, respectively, according to their Levin–Halperin daughters. (**C-F**) R_{xx} measurements near the four quarter-filled states. White dots in (E) mark the values of D where we measured the gap $\Delta_{\frac{3}{4}}$ in Fig 4E.

Upon tuning the orbital index from $N = 1$ to $N = 0$, we observed quarter-filled states at $\nu = \frac{3}{4} + (-4, -2, 0, +2)$ and a suppression of the ^{4}CF Jain sequences around these fillings. The systematic occurrence of these states at every second level suggests a common origin. Additionally, we find daughter states at $\nu = \frac{9}{25} + (-4, -2, 0)$ but not at $\nu = \frac{9}{25} + 2$; see Fig. 2C–F.

In Fig. 2B, we summarize the observed quarter- and half-filled states along with their daughter states, highlighting their dependence on the orbital and valley isospin indices. The newly found half- and quarter-filled states are shown by bold, solid black lines. We already labeled the even-denominator states according to their identification via Levin–Halperin daughter states and in-plane B measurements, which we discuss below.

We proceed with a detailed characterization of all half-filled states. To avoid ambiguity, we identify all states according to the topological phase of the *electrons* for either sign of ν. In Fig. 3A, we show the filling factors of daughters associated with different pairing channels of ^{2}CFs.[38,39] In Fig. 3B, we show R_{xx} and R_{xy} around $\nu = \frac{1}{2}$ at $D = -140\ \mathrm{mV/nm}$, with strong dips in R_{xx} flanking the plateau at half filling. The absence of higher-order Jain states beyond $\nu = \frac{2}{5}, \frac{3}{5}$ suggests that the dips near $\nu = \frac{1}{2}$ are daughter states. We mark possible daughter-state fillings by vertical lines for the most relevant pairing channels, including Moore–Read and anti-Pfaffian favored by numerics[3] and PH-Pfaffian indicated by thermal measurements in GaAs.[49–51] The observed dips coincide with $\frac{6}{13}$ and $\frac{9}{17}$, supporting anti-Pfaffian pairing for $\nu = \frac{1}{2}$. Our analysis of the other half-filled states and the plateaus of their daughters, which agrees with previous reports,[22] is shown in SM Sec. 8–10. The identification of paired states based on their daughters is indirect and has not been independently confirmed by direct measurements, such as thermal conductance[49,50] or upstream noise at interfaces[51]. Still, the periodic pattern of topological orders indicated by daughters[38,39] and its systematic association with crossing $N = 1$ levels provides strong support for its veracity.

Fig. 3C shows the dependence of the gap $\Delta_{\nu=\frac{1}{2}}$ on an in-plane magnetic field $B_\parallel$ at an out-of-plane field of $B_\perp = 15\ \mathrm{T}$ (see SM Sec. 7 for more details). We observe only negligible variations of $\Delta_{\frac{1}{2}}$ up to the largest accessible value of $B_\parallel = 10\ \mathrm{T}$ and conclude that the $\nu = \frac{1}{2}$ state is fully spin-polarized, as expected for the anti-Pfaffian. A detailed characterization of $\nu = -\frac{3}{2}$ also indicates a spin-polarized state; see SM Sec. 10.



E

filling factor	activation gap (K)	parent state
3 + 1/2	3.10 ± 0.25	Pfaffian
3 + 8/17, 7/13	≲ 0.17, ≲ 0.18	
2 + 1/2	1.10 ± 0.10	anti-Pfaffian
2 + 6/13, 9/17	≲ 0.18 , ≲ 0.10	
1 + 1/2	3.60 ± 0.40	Pfaffian
1 + 8/17, 7/13	(0.18 ± 0.06) , (0.53 ± 0.1)	
0 + 1/2	1.87 ± 0.12	anti-Pfaffian
0 + 6/13, 9/17	≲ 0.15 , ≲ 0.13	
- 1 + 1/2	2.58 ± 0.11	Pfaffian
- 1 + 8/17, 7/13	(0.25 ± 0.03) , (0.38 ± 0.08)	
- 2 + 1/2	0.50 ± 0.05 @ 11.2T	anti-Pfaffian
- 2 + 6/13, 9/17	≲ 0.10 , ≲ 0.10 @ 11.2T	
- 3 + 1/2	1.74 ± 0.13	Pfaffian
- 3 + 8/17, 7/13	≲ 0.12 , ≲ 0.20	

parent state
daughter states

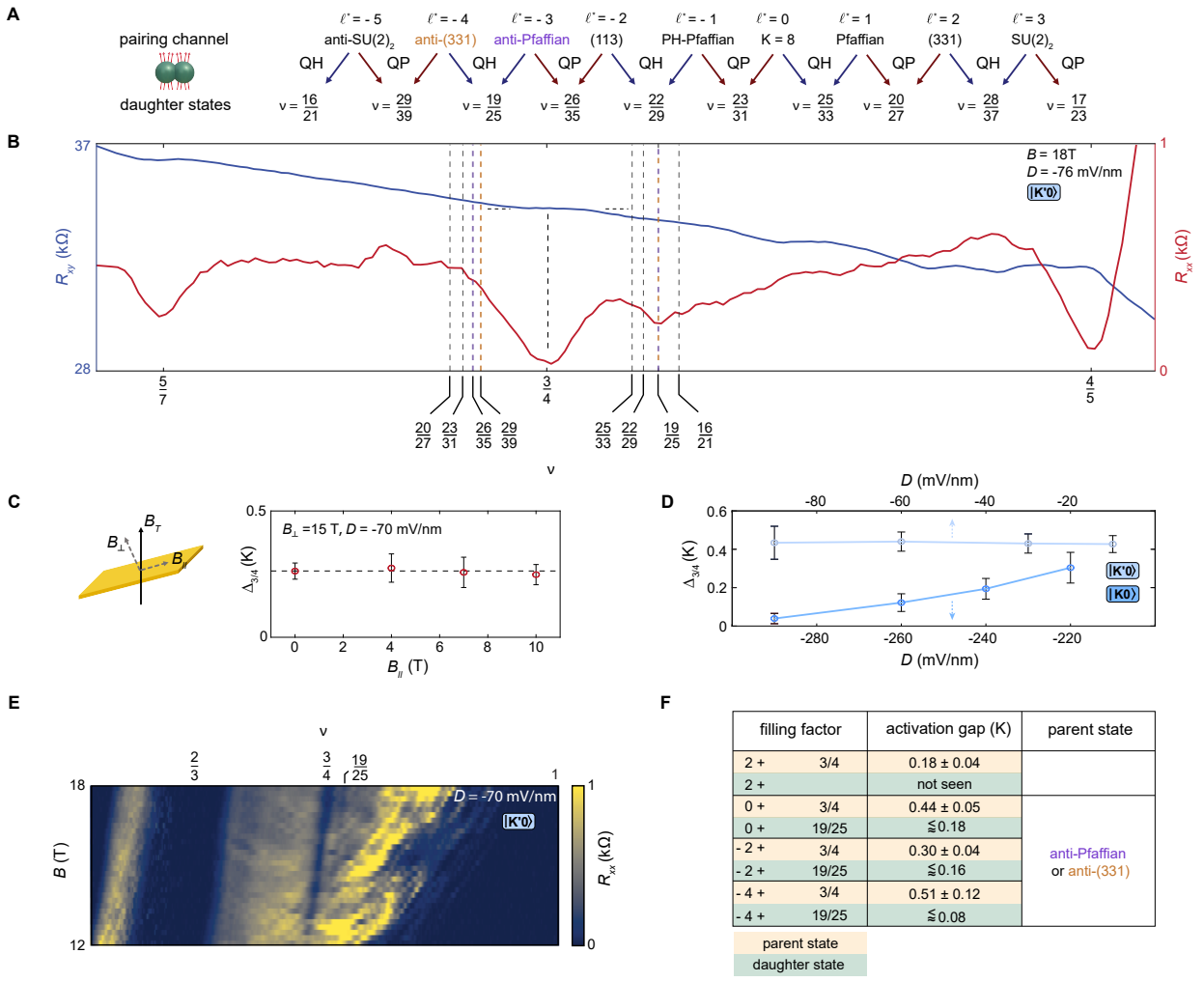
Figure 3: Topological orders of half-filled states in BLG. (**A**) Classification of half-filled states and their identification based on daughter-state fillings. The pairing channel ℓ corresponds to the number of Majorana edge channels (see SM Sec. 13). (**B**) R_{xx} and R_{xy} around $\nu = \frac{1}{2}$, measured at $B = 18$ T and $D = -140$ mV/nm, along with possible daughter states marked by vertical dashed lines. (**C**) The thermal activation gap $\Delta_{\frac{1}{2}}$ measured as a function of $B_\parallel$ at $B_\perp = 15$ T. (**D**) R_{xx} around $\nu = \frac{3}{2}$ measured as a function of B for $D = -140$ mV/nm. (**E**) Identification of all observed half-filled states based on their daughters, along with the measured thermal activation gaps. The gap of all the half-filled states was measured at $B = 18$ T, except for $\nu = -\frac{3}{2}$ which was measured at $B = 11.2$ T.

We summarize our identification of the half-filled states in the table of Fig. 3E (see SM Secs. 5 and 8 for gap measurements and daughters of other half-filled states). Strikingly, all observed anti-Pfaffians (aPf) occur in a pair with a Pfaffian (Pf) in the vicinity of crossing $N = 1$ levels. There is one such crossing for $(-\frac{3}{2},-\frac{1}{2})$, two for $(\frac{1}{2},\frac{3}{2})$, and one for $(\frac{5}{2},\frac{7}{2})$, each exhibiting (aPf, Pf) on both sides of the crossing. This observation suggests that Landau-level mixing within these pairs is most relevant for determining the

topological order at half filling. Pfaffian or anti-Pfaffian are favored by Landau-level mixing,[52–54] which is opposite for the two members of each pair. In the lower one, electrons can virtually occupy the empty level above; in the upper one, holes can virtually occupy the filled level below. By contrast, the spin and valley isospin appear to play subordinate roles. The largest gap occured at $\nu = \frac{3}{2}$. Fig. 3D shows R_{xx} near this filling as a function of ν and B. The incompressible state at $\nu = \frac{3}{2}$ persists down to $B = 6$ T, which places half-filled states in BLG within reach of commonly available magnetic-field setups.

We turn to a detailed analysis of the quarter-filled states. Similar to their cousins at half filling, quarter states can also exhibit characteristic daughters.[38] In Fig. 4A, we show the filling factors of daughters associated with the main pairing channels. In Fig. 4B, we show R_{xx} and R_{xy} around $\nu = \frac{3}{4}$ with the possible daughter states indicated by dashed lines.

The state at $\nu = \frac{19}{25}$ shows remarkable agreement with our data, thereby constraining the $\nu = \frac{3}{4}$ topological order to either the non-Abelian anti-Pfaffian or the Abelian anti-(331). To determine the spin polarization of the $\nu = \frac{3}{4}$ state, we measured its gap while varying $B_\parallel$ at $B_\perp = 15$ T; see Fig. 4C and SM Sec. 7 for more details. The weak dependence of $\Delta_{\frac{3}{4}}$ on $B_\parallel$ indicates a fully spin-polarized state. In conjunction with the observed daughter state, this observation supports the non-Abelian anti-Pfaffian ground state, as the spin-singlet anti-(331) state should not be spin-polarized.[55] However, a valley-singlet anti-(331) state remains possible.



filling factor		activation gap (K)	parent state
2 +	3/4	0.18 ± 0.04	
2 +		not seen	
0 +	3/4	0.44 ± 0.05	
0 +	19/25	≲0.18	
- 2 +	3/4	0.30 ± 0.04	anti-Pfaffian or anti-(331)
- 2 +	19/25	≲0.16	
- 4 +	3/4	0.51 ± 0.12	
- 4 +	19/25	≲0.08	

Figure 4: Quarter-filled states in BLG. (**A**) Classification of quarter-filled states and their identification based on daughter-state fillings. The pairing channel ℓ corresponds to the number of Majorana edge channels (see SM Sec. 13). (**B**) R_{xx} and R_{xy} around $\nu = \frac{3}{4}$ measured at $D = -76\ \mathrm{mV/nm}$, along with possible daughter states marked by vertical dashed lines. (**C**) The thermal activation gap of $\nu = \frac{3}{4}$ measured as a function of $B_{\parallel}$ at $B_{\perp} = 15$ T. (**D**) $\Delta_{\frac{3}{4}}$ measured as a function of D in different valleys. (**E**) R_{xx} around $\nu = \frac{3}{4}$ measured as a function of B for $D = -70\ \mathrm{mV/nm}$. (**F**) Constraints on the ground states of all observed quarter-filled states based on their daughters, along with the measured thermal activation gaps.

To probe the valley polarization, we measured $\Delta_{\frac{3}{4}}$ as a function of D; see Fig. 4D and SM Sec. 6 for more details. For the K' valley, we find that the gap remains constant as the absolute value of D increases. By contrast, in the K valley, the gap decreases monotonically. However, this behavior does not necessarily imply a valley singlet state. Indeed, a reduction of the gap with D was also reported for $\nu = \frac{3}{2}$.[18] There, the gap eventually saturates to a non-zero value, and a single-component state is further supported by the

daughters.[22] Consequently, our measurement can neither rule out an anti-Pfaffian nor a valley-singlet anti-(331) state. Fig. 4E shows R_{xx} as a function of ν and B, with the incompressible state at $\nu = \frac{3}{4}$ persisting down to $B = 12$ T. We summarize our analysis of all observed quarter-filled states and their daughters in the table of Fig. 4F (see SM Secs. 5 and 8 for gap measurements and daughters of other quarter-filled states).

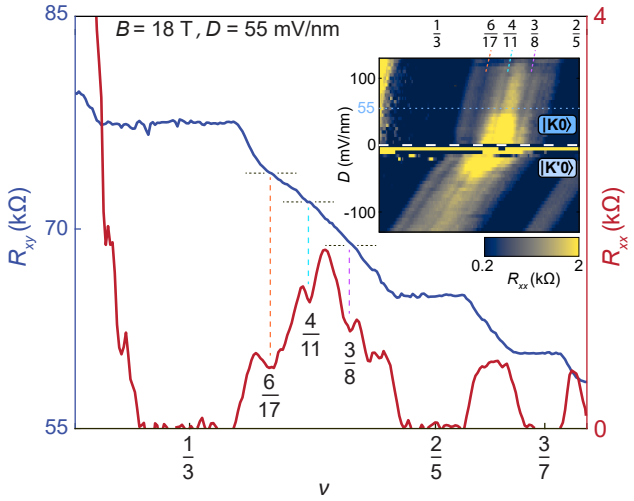


Figure 5: Odd- and even-denominator FQH states in partially filled Landau levels of ^{2}CFs. R_{xx} and R_{xy} measured at $B = 18$ T and $D = 55$ mV/nm between $\nu = \frac{1}{3}$ and $\frac{3}{7}$. Dashed vertical and horizontal lines mark the minima in R_{xx} and plateaus in R_{xy}, respectively. The electron fillings $\nu = \frac{6}{17}, \frac{4}{11}, \frac{3}{8}$ correspond to ^{2}CFs at fillings $\nu_{\mathrm{CF}} = \frac{4}{3}, \frac{6}{5}$, and $\frac{3}{2}$, respectively. The magnified region in the inset is indicated in Fig. 2A and shows R_{xx} as a function of ν and D. The dotted blue line marks the R_{xx} line cut at $D = 55$ mV/nm.

Finally, we have also observed 'next-generation' FQH states, which are not captured by weakly interacting CFs.[32,46,56–58] In Fig. 5, we show R_{xx} and R_{xy} at $D = 55$ mV/nm from $\frac{1}{3} \leq \nu \leq \frac{3}{7}$, identifying two odd-denominator states $\nu = \frac{4}{11}$ and $\nu = \frac{6}{17}$ as well as the even denominator $\nu = \frac{3}{8}$ (see SM Sec. 11 for additional next-generation states). They predominantly form in the $N = 0$ orbital, similar to the paired ^{4}CF states at $\nu = \frac{3}{4}$. We note that the $\nu = \frac{3}{4}$ states can also be viewed as FQH states of ^{2}CFs at $\nu_{\mathrm{CF}} = -\frac{3}{2}$,[32] see also SM Sec. 13. These observations suggest that the $N = 0$ levels of BLG favor the formation of FQH states of ^{2}CFs.

Conclusion. We uncovered a systematic and universal manner in which the topological orders of half-filled FQH states in BLG are determined. Near crossings of two $N = 1$ levels, we consistently find (aPf, Pf) in the lower and upper levels, respectively, suggesting that Landau-level mixing within these pairs is decisive. Additionally, we have observed four systematically occurring paired states of ^{4}CFs and constrained their topological order based on daughter states to be of either anti-Pfaffian or anti-(331) order. The quarter-

filled states arise exclusively in $N = 0$ orbitals, oppositely to the half-filled states, which occur at $N = 1$. Moreover, the $N = 0$ orbitals also host 'next-generation' odd- and even-denominator FQH states, previously only observed in GaAs[46,56,58,59] and in suspended monolayer graphene.[60]

Our work highlights two arenas of competing CF interactions. First, their pairing competes against the formation of integer quantum Hall states of CFs, i.e., the Jain sequence. Second, interactions favoring the pairing of ^{2}CFs disfavor pairing of ^{4}CFs and vice versa. Both competitions can be observed and manipulated electrostatically in a single BLG heterostructure.

References

1. Read, N. & Green, D. Paired states of fermions in two dimensions with breaking of parity and time-reversal symmetries and the fractional quantum Hall effect. *Phys. Rev. B* **61**, 10267 (2000).

2. Willett, R. *et al.* Observation of an even-denominator quantum number in the fractional quantum Hall effect. *Phys. Rev. Lett.* **59**, 1776 (1987).

3. Ma, K. K., Peterson, M. R., Scarola, V. & Yang, K. Fractional quantum Hall effect at the filling factor $\nu = 5/2$. *Encyclopedia of Condensed Matter Physics 2nd ed. Vol. 1* 324–365 (2024).

4. Moore, G. & Read, N. Nonabelions in the fractional quantum Hall effect. *Nucl. Phys. B* **360**, 362 (1991).

5. Greiter, M., Wen, X. G. & Wilczek, F. Paired Hall state at half filling. *Phys. Rev. Lett.* **66**, 3205 (1991).

6. Lee, S. S., Ryu, S., Nayak, C. & Fisher, M. P. A. Particle-Hole Symmetry and the $\nu = 5/2$ Quantum Hall state. *Phys. Rev. Lett.* **99**, 236807 (2007).

7. Levin, M., Halperin, B. I. & Rosenow, B. Particle-Hole Symmetry and the Pfaffian State. *Phys. Rev. Lett.* **99**, 236806 (2007).

8. Son, D. T. Is the Composite Fermion a Dirac Particle? *Phys. Rev. X* **5**, 031027 (2015).

9. Halperin, B. Theory of the quantized Hall conductance. *Helv. Phys. Acta* 75 (1983).

10. Halperin, B. I., Lee, P. A. & Read, N. Theory of the half-filled Landau level. *Phys. Rev. B* **47**, 7312 (1993).

11. Suen, Y., Engel, L., Santos, M., Shayegan, M. & Tsui, D. Observation of a $\nu = 1/2$ fractional quantum Hall state in a double-layer electron system. *Phys. Rev. Lett.* **68**, 1379 (1992).

12. Eisenstein, J., Boebinger, G., Pfeiffer, L., West, K. & He, S. New fractional quantum Hall state in double-layer two-dimensional electron systems. *Phys. Rev. Lett.* **68**, 1383 (1992).

13. Suen, Y., Manoharan, H., Ying, X., Santos, M. & Shayegan, M. Origin of the $\nu = 1/2$ fractional quantum Hall state in wide single quantum wells. *Phys. Rev. Lett.* **72**, 3405 (1994).

14. Shabani, J. *et al.* Phase diagrams for the stability of the $\nu = 1/2$ fractional quantum Hall effect in electron systems confined to symmetric, wide GaAs quantum wells. *Phys. Rev. B* **88**, 245413 (2013).

15. Falson, J. *et al.* Even-denominator fractional quantum Hall physics in ZnO. *Nat. Phys.* **11**, 347–351 (2015).

16. Singh, S. *et al.* Topological phase transition between Jain states and daughter states of the $\nu = 1/2$ fractional quantum Hall state. *Nature Physics* 1–6 (2024).

17. Ki, D. K., Fal'ko, V. I., Abanin, D. A. & Morpurgo, A. F. Observation of Even Denominator Fractional Quantum Hall Effect in Suspended Bilayer Graphene. *Nano Lett.* **14**, 2135–2139 (2014).

18. Li, J. *et al.* Even-denominator fractional quantum hall states in bilayer graphene. *Science* **358**, 648–652 (2017).

19. Zibrov, A. A. *et al.* Tunable interacting composite fermion phases in a half-filled bilayer-graphene Landau level. *Nature* **549**, 360–364 (2017).

20. Kim, Y. *et al.* Even denominator fractional quantum hall states in higher landau levels of graphene. *Nat. Phys.* **15**, 154–158 (2019).

21. Shi, Q. *et al.* Odd- and even-denominator fractional quantum Hall states in monolayer WSe_2. *Nat. Nanotechnol.* **15**, 569–573 (2020).

22. Huang, K. *et al.* Valley Isospin Controlled Fractional Quantum Hall States in Bilayer Graphene. *Phys. Rev. X* **12**, 031019 (2022). Erratum: *Phys. Rev. X* **12**, 049901 (2022).

23. Chen, Y. *et al.* Tunable even-and odd-denominator fractional quantum hall states in trilayer graphene. *Nature Communications* **15**, 6236 (2024).

24. Jain, J. K. Composite-fermion approach for the fractional quantum Hall effect. *Phys. Rev. Lett.* **63**, 199 (1989).

25. Morf, R. H. Transition from quantum Hall to compressible states in the second Landau level: new light on the $\nu = 5/2$ enigma. *Phys. Rev. Lett.* **80**, 1505 (1998).

26. Zhang, F. C. & Das Sarma, S. Excitation gap in the fractional quantum Hall effect: Finite layer thickness corrections. *Phys. Rev. B* **33**, 2903–2905 (1986).

27. Papić, Z., Möller, G., Milovanović, M. V., Regnault, N. & Goerbig, M. O. Fractional quantum Hall state at $\nu = \frac{1}{4}$ in a wide quantum well. *Phys. Rev. B* **79**, 245325 (2009).

28. Luhman, D. R. *et al.* Observation of a Fractional Quantum Hall State at $\nu = 1/4$ in a Wide GaAs Quantum Well. *Phys. Rev. Lett.* **101**, 266804 (2008).

29. Shabani, J., Gokmen, T., Chiu, Y. T. & Shayegan, M. Evidence for Developing Fractional Quantum Hall States at Even Denominator $1/2$ and $1/4$ Fillings in Asymmetric Wide Quantum Wells. *Phys. Rev. Lett.* **103**, 256802 (2009).

30. Shabani, J., Gokmen, T. & Shayegan, M. Correlated States of Electrons in Wide Quantum Wells at Low Fillings: The Role of Charge Distribution Symmetry. *Phys. Rev. Lett.* **103**, 046805 (2009).

31. Wang, C. *et al.* Even-Denominator Fractional Quantum Hall State at Filling Factor $\nu = 3/4$. *Phys. Rev. Lett.* **129**, 156801 (2022).

32. Wang, C. *et al.* Next-generation even-denominator fractional quantum Hall states of interacting composite fermions. *Proc. Natl. Acad. Sci. U.S.A.* **120**, e2314212120 (2023).

33. Zibrov, A. A. *et al.* Even-denominator fractional quantum Hall states at an isospin transition in monolayer graphene. *Nat. Phys.* **14**, 930–935 (2018).

34. Zhao, T., Balram, A. C. & Jain, J. K. Composite Fermion Pairing Induced by Landau Level Mixing. *Phys. Rev. Lett.* **130**, 186302 (2023).

35. Sharma, A., Balram, A. C. & Jain, J. K. Composite-fermion pairing at half-filled and quarter-filled lowest Landau level. *Phys. Rev. B* **109**, 035306 (2024).

36. Jain, J. K. Incompressible quantum Hall states. *Phys. Rev. B* **40**, 8079–8082 (1989).

37. Levin, M. & Halperin, B. I. Collective states of non-Abelian quasiparticles in a magnetic field. *Phys. Rev. B* **79**, 205301 (2009).

38. Yutushui, M., Hermanns, M. & Mross, D. F. Paired fermions in strong magnetic fields and daughters of even-denominator Hall plateaus. *arXiv e-prints* arXiv:2405.03753 (2024).

39. Zheltonozhskii, E., Stern, A. & Lindner, N. Identifying the topological order of quantized half-filled Landau levels through their daughter states. *arXiv e-prints* arXiv:2405.03780 (2024).

40. Zhou, H. *et al.* Isospin magnetism and spin-polarized superconductivity in Bernal bilayer graphene. *Science* **375**, 774–778 (2022).

41. McCann, E. & Fal'ko, V. I. Landau-Level Degeneracy and Quantum Hall Effect in a Graphite Bilayer. *Phys. Rev. Lett.* **96**, 086805 (2006).

42. Hunt, B. M. *et al.* Direct measurement of discrete valley and orbital quantum numbers in bilayer graphene. *Nat. Commun.* **8**, 948 (2017).

43. Kousa, B. M., Wei, N. & MacDonald, A. H. Orbital Competition in Bilayer Graphene's Fractional Quantum Hall Effect. *arXiv preprint arXiv:2402.10440* (2024).

44. Assouline, A. *et al.* Energy Gap of the Even-Denominator Fractional Quantum Hall State in Bilayer Graphene. *Phys. Rev. Lett.* **132**, 046603 (2024).

45. Smet, J. H. Wheels within wheels. *Nature* **422**, 391–392 (2003).

46. Chang, C.-C. & Jain, J. K. Microscopic Origin of the Next-Generation Fractional Quantum Hall Effect. *Phys. Rev. Lett.* **92**, 196806 (2004).

47. Scarola, V. W., Park, K. & Jain, J. K. Cooper instability of composite fermions. *Nature* **406**, 863–865 (2000).

48. Pizzocchero, F. *et al.* The hot pick-up technique for batch assembly of van der Waals heterostructures. *Nat. Commun.* **7**, 11894 (2016).

49. Banerjee, M. *et al.* Observation of half-integer thermal Hall conductance. *Nature* **559**, 205 (2018).

50. Dutta, B., Umansky, V., Banerjee, M. & Heiblum, M. Isolated ballistic non-Abelian interface channel. *Science* **377**, 1198–1201 (2022).

51. Dutta, B. *et al.* Distinguishing between non-Abelian topological orders in a quantum Hall system. *Science* **375**, 193–197 (2022).

52. Rezayi, E. H. & Simon, S. H. Breaking of Particle-Hole Symmetry by Landau Level Mixing in the $\nu = 5/2$ Quantized Hall State. *Phys. Rev. Lett.* **106**, 116801 (2011).

53. Pakrouski, K. *et al.* Phase Diagram of the $\nu = 5/2$ Fractional Quantum Hall Effect: Effects of Landau-Level Mixing and Nonzero Width. *Phys. Rev. X* **5**, 021004 (2015).

54. Rezayi, E. H. Landau Level Mixing and the Ground State of the $\nu = 5/2$ Quantum Hall Effect. *Phys. Rev. Lett.* **119**, 026801 (2017).

55. Haldane, F. D. M. Fractional quantization of the Hall effect: A hierarchy of incompressible quantum fluid states. *Phys. Rev. Lett.* **51**, 605 (1983).

56. Pan, W. *et al.* Fractional quantum Hall effect of composite fermions. *Phys. Rev. Lett.* **90**, 016801 (2003).

57. Wójs, A., Yi, K.-S. & Quinn, J. J. Fractional quantum Hall states of clustered composite fermions. *Phys. Rev. B* **69**, 205322 (2004).

58. Pan, W., Baldwin, K., West, K., Pfeiffer, L. & Tsui, D. Fractional quantum Hall effect at Landau level filling $\nu = 4/11$. *Phys. Rev. B* **91**, 041301 (2015).

59. Samkharadze, N., Arnold, I., Pfeiffer, L., West, K. & Csáthy, G. Observation of incompressibility at $\nu = 4/11$ and $\nu = 5/13$. *Phys. Rev. B* **91**, 081109 (2015).

60. Kumar, M., Laitinen, A. & Hakonen, P. Unconventional fractional quantum Hall states and Wigner crystallization in suspended Corbino graphene. *Nat. Commun.* **9**, 2776 (2018).

61. Purdie, D. G. *et al.* Cleaning interfaces in layered materials heterostructures. *Nat. Commun.* **9**, 5387 (2018).

62. Wang, L. *et al.* One-dimensional electrical contact to a two-dimensional material. *Science* **342**, 614–617 (2013).

Materials and Methods

The heterostructure was fabricated using the well-known dry-transfer stacking technique.[48] The flakes of hexagonal boron nitride (hBN), BLG, and few-layer graphite for the gates were exfoliated on a silicon substrate with a 285-nm SiO_2 layer. A polydimethylsiloxane stamp covered with polycarbonate (PC) was used to pick up the top graphite flake and then, subsequently, hBN, BLG, hBN, and bottom graphite flakes from the substrate. The heterostructure, along with the PC film, was then landed on a clean substrate of the same kind. The substrate was cleaned in chloroform for two hours to remove residual PC. The heterostructure was then vacuum-annealed at $400°\mathrm{C}$ for three hours and an AFM was used to clean the stack[61] and determine the thicknesses of individual flakes. The desired geometry was achieved by dry-etching (O_2 for graphite gates, CHF_3/O_2 for hBN)[62] and, finally, contacts were deposited (2–3 nm chromium, $13\ \mathrm{nm}$ palladium, $70\ \mathrm{nm}$ gold). After deposition, a lift-off procedure was performed in acetone and IPA. The final device's optical image is shown in Fig. S1A. Four-probe resistance measurements were performed using the standard lock-in technique. An illustration of the measurement scheme is shown in SM Fig. S1B.

All measurements were performed in the n–D phase space with the desired values converted to top and bottom gate voltages according to

$$V_{\mathrm{tg}} = \frac{d_{\mathrm{hBN,top}}}{\varepsilon_{\mathrm{hBN}}}\left(\frac{ne}{2\varepsilon_0} - D\right) + V_{\mathrm{CNP,top}},$$
$$V_{\mathrm{bg}} = \frac{d_{\mathrm{hBN,bottom}}}{\varepsilon_{\mathrm{hBN}}}\left(\frac{ne}{2\varepsilon_0} + D\right) + V_{\mathrm{CNP,bottom}},$$

where $d_{\mathrm{hBN,(top,bottom)}}$ are the top and bottom hBN thicknesses, $\varepsilon_{\mathrm{hBN}} = 3.9$ is the dielectric constant of hBN, and $V_{\mathrm{CNP,(top,bottom)}}$ is the top and bottom gate voltage corresponding to the charge-neutrality point of the device.

The device geometry reveals the origin of meandering artifacts in our R_{xx} data. Due to the placement of the different gates, we obtain several interfaces at the edge: From the actual Cr/Pd/Au contact to a silicon-gated region onto another region that is gated by the graphite top gate and the silicon gate and then the actual device. At negative (positive) D on the hole (electron) side, the silicon bottom gate is at a negative (positive) voltage, and the graphite top gate is at a positive (negative) voltage, thus depleting the contact region of charge carriers, resulting in large contact resistance and, eventually, the artifacts seen in our R_{xx} data.

Data and materials availability:

The data supporting the plots in this paper and other findings of this study are available from the corresponding author upon request.

Acknowledgements

It is a pleasure to thank Moty Heiblum and Mike Zaletel for illuminating discussions. **Funding:** R.K. acknowledges support from the Dean of the Faculty and the Clore Foundation. Y.R. acknowledges the support from the Quantum Science and Technology Program 2021, the Schwartz Reisman Collaborative Science Program, supported by the Gerald Schwartz and Heather Reisman Foundation, the Minerva Foundation with funding from the Federal German Ministry for Education and Research, and the European Research Council Starting Investigator Grant Anyons 101163917. D.F.M. acknowledges support from the Israel Science Foundation (ISF) under grant 2572/21 and from the Minerva Foundation with funding from the Federal German Ministry for Education and Research.

Author contributions

R.K. fabricated the device. R.K., J.K., K.K., V.B, and A.I. helped in improving the device quality. K.W. and T.T. grew the hBN crystals. A.H. developed the measurement codes. R.K. and A.H. performed the measurements. R.K., A.H., M.Y., D.F.M., and Y.R. analyzed the measured data. M.Y. and D.F.M. developed the theoretical aspect. R.K., A.H., M.Y., D.F.M., and Y.R. authored the paper with input from all coauthors. Y.R. supervised the overall work done on the project.

Competing interests

The authors declare no competing interests.

Supplementary material for Quarter- and half-filled quantum Hall states and their competing interactions in bilayer graphene

This supplementary information contains the following details:

1. Device optical image and measurement schematic

2. Device characterization at $0\ \mathrm{T}$

3. R_{xx} **versus** ν **and** B

4. R_{xx} **versus** ν **and** D

5. Thermally activated transport measurements

6. Energy gap of $\nu = \frac{3}{4}$ **in different valleys**

7. In-plane magnetic-field measurements

8. All other half- and quarter-filled states and their daughters

9. Quantized plateaus at daughter state filling

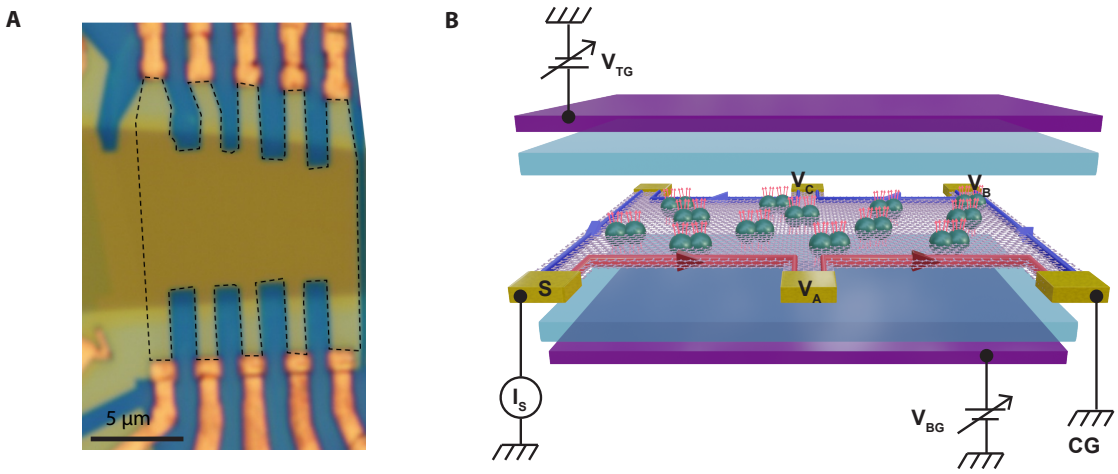
10. Half-filled state at $\nu = -\frac{3}{2}$

11. Next-generation FQH states

12. Data from device 2

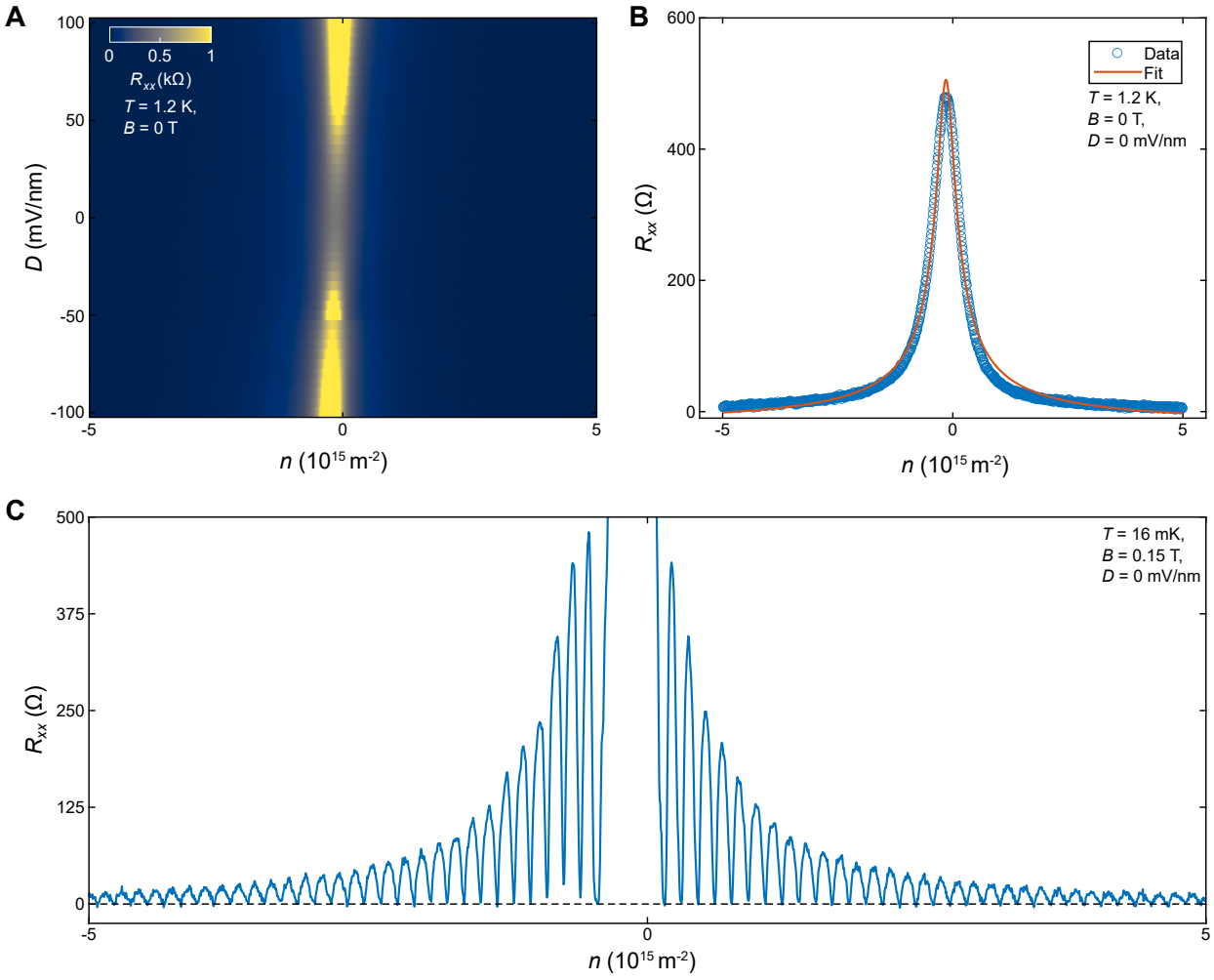
13. Paired composite-fermion states at $\nu = \frac{3}{4}$

Section S1: Device optical image and measurement schematic



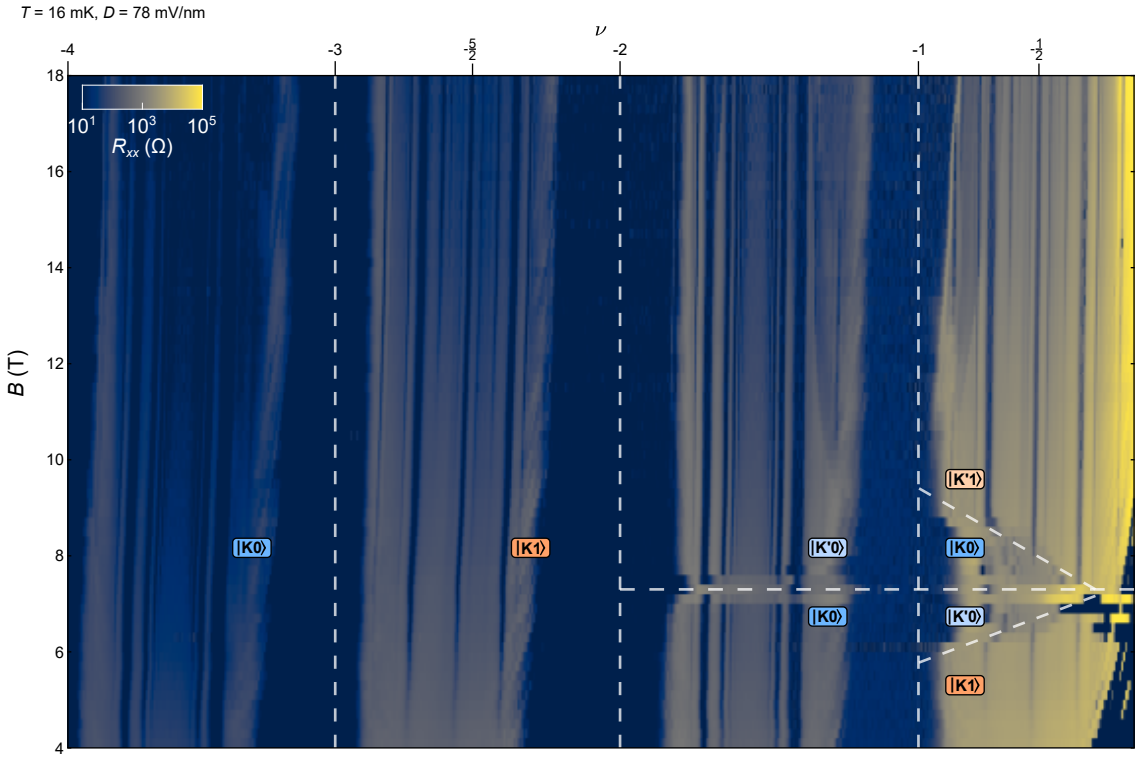
Supplementary Figure 1: Device. **(A)** Optical image of device 1, where the black dashed line outlines the bilayer graphene. **(B)** Illustration of our 5-layer heterostructures consisting of graphite/hBN/BLG/hBN/graphite on top of a silicon substrate with a 285-nm SiO_2 layer (not shown). The four-flux composite fermions symbolically indicate the formation of a paired quantum Hall state. A constant AC current, I_S, is injected at the source contact **S** and drained into the cold ground (CG) contact. Red and blue arrows indicate hot and cold edges, respectively. The transverse and longitudinal voltages are obtained by measuring $V_A - V_B$ and $V_B - V_C$, respectively.

Section S2: Device characterization at 0 T

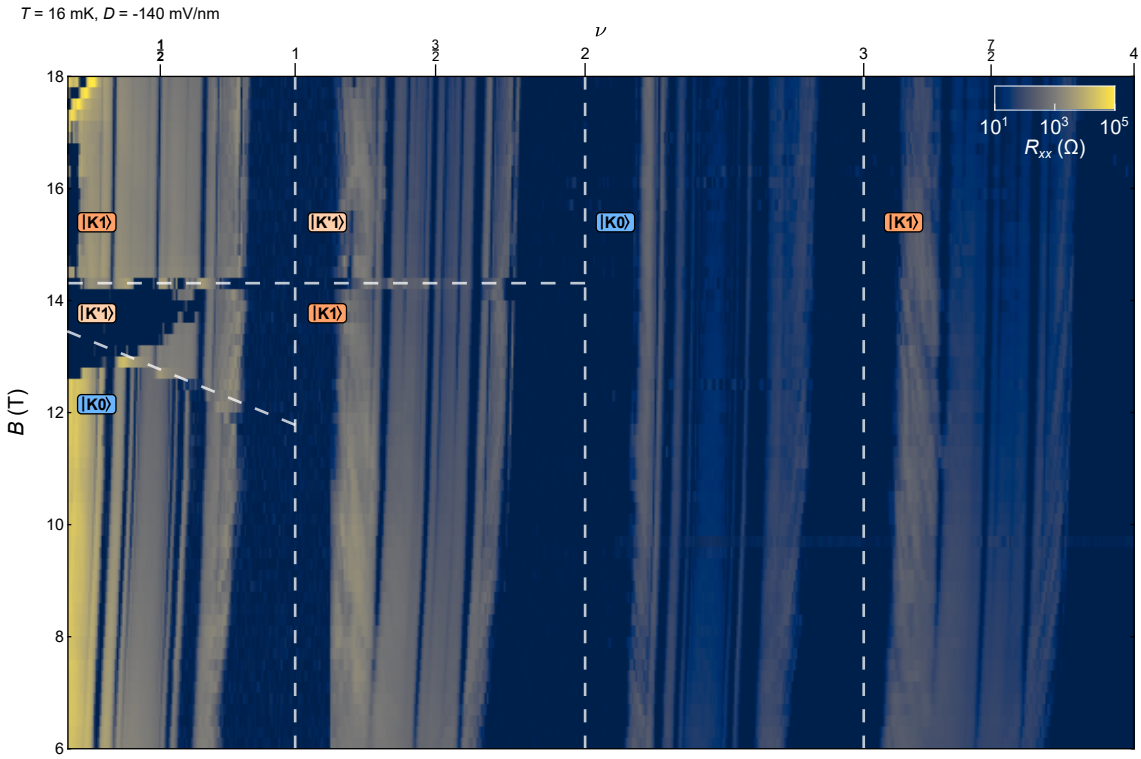


Supplementary Figure 2: Characterization of device 1. (**A**) R_{xx} versus n and D at $T = 1.2$ K, $B = 0$. We observe the opening of a gap at charge neutrality as D is increased at $B = 0$, as expected for BLG. (**B**) R_{xx} versus n at $D = 0$ mV/nm, $B = 0$ T. From the fit $R_{xx} = a + \frac{L}{We\mu\sqrt{(n-n_0)^2+c^2}}$, with $L/W \approx 0.3$ and the parameters μ, n_0, and c, we obtain an electron mobility of $\mu \approx 1.8 \times 10^5$ cm^2/Vs. (**C**) R_{xx} versus n at $D = 0$ mV/nm, $B = 0.15$ T. The strong SdH oscillations at such a low B again highlight the device quality. The minima in R_{xx} are equally spaced and reflect the fourfold degenerate higher LLs in BLG.

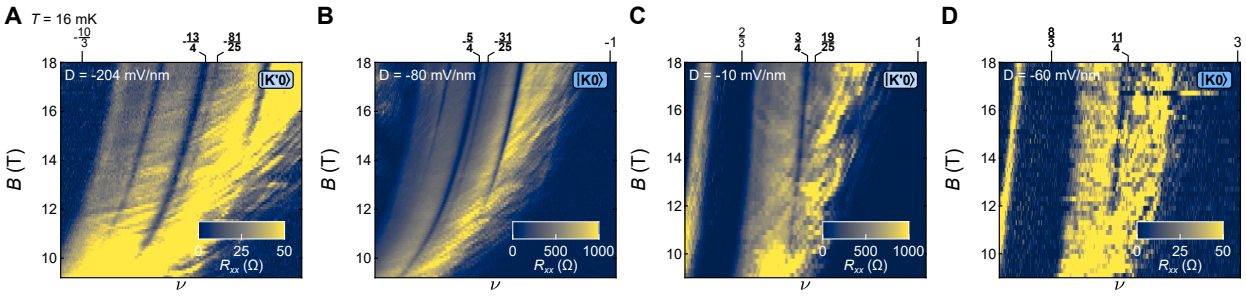
Section S3: R_{xx} versus ν and B



Supplementary Figure 3: R_{xx} as a function of ν and B on the hole side at $D = 78\ \mathrm{mV/nm}$. Around $B \approx 7\ \mathrm{T}$, there is a sequence of transitions from $K'1 \to K0 \to K'0 \to K1$ at $-1 < \nu < 0$. After the first transition, the $\nu = -\frac{1}{2}$ state is replaced by a compressible state with SdH oscillations and reappears upon entering $K1$. Eventually, $\nu = -\frac{1}{2}$ vanishes at a field as low as $\sim 4\ \mathrm{T}$. A similar transition $K0 \to K'0$ occurs at $-2 < \nu < -1$. The even-denominator state visible at $D = 78\ \mathrm{mV/nm}$ with filling $\nu = -\frac{5}{2}$ disappears between 4 and $5\ \mathrm{T}$.

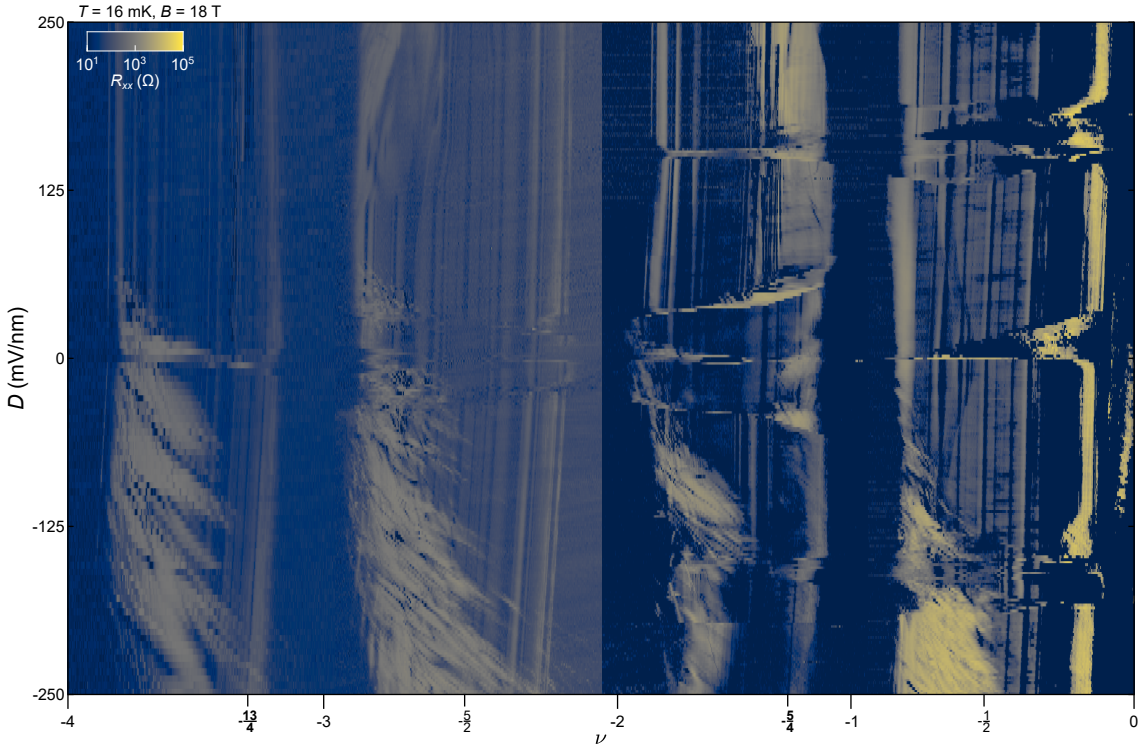


Supplementary Figure 4: R_{xx} as a function of ν and B on the electron side at $D = -140\ \mathrm{mV/nm}$. At $0 < \nu < 1$, there is a sequence of transitions $K1 \rightarrow K'1 \rightarrow K0$ as B decreases. The horizontal line spanning $0 < \nu < 2$ is the transition from $K1$ ($K'1$) to $K'1$ ($K1$) at $0 < \nu < 1$ ($1 < \nu < 2$). Around $B = 13$ T, the $\nu = \frac{1}{2}$ state disappears and is replaced by SdH oscillations. We stress that this is due to the transition to the $N = 0$ orbital and not due to small B. At higher ν, we see even-denominator states persisting down to below 6 T.

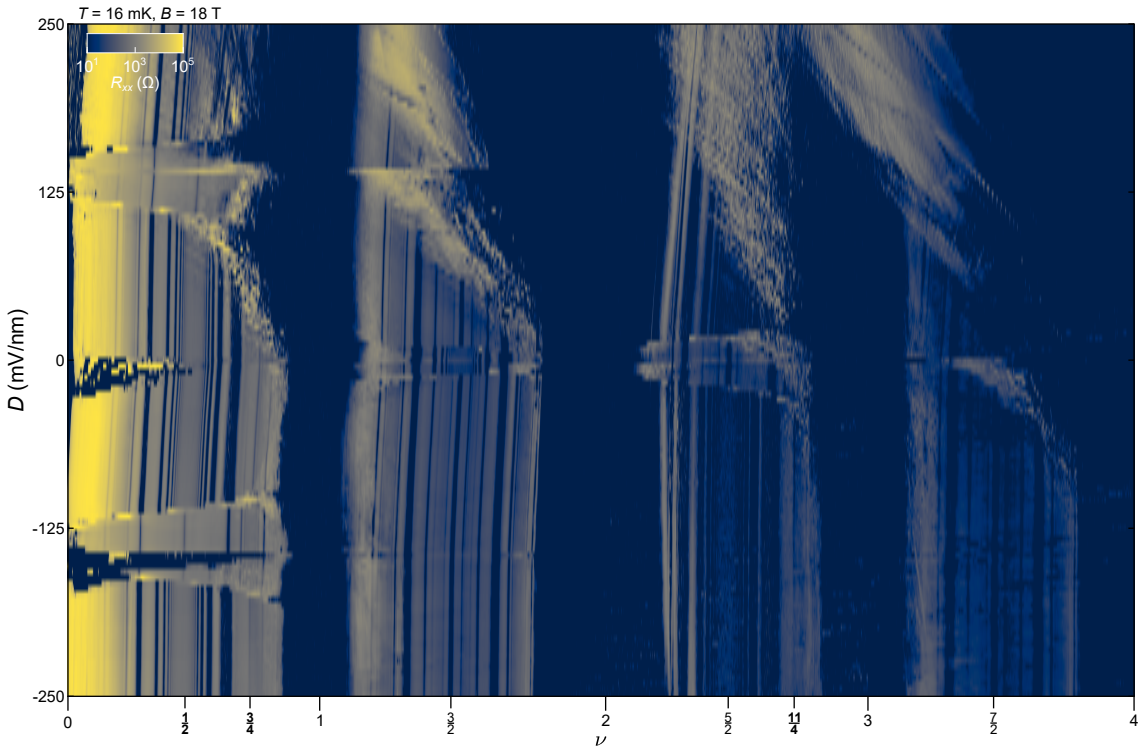


Supplementary Figure 5: R_{xx} versus ν and B for the quarter-filled states.

Section S4: R_{xx} versus ν and D



Supplementary Figure 6: R_{xx} as a function of ν and D from $\nu = -4$ to 0. Data from -4 to -2 are hot R_{xx}, data from -2 to 0 are cold R_{xx}, hence the difference in minimum R_{xx}. Larger version of the hole side of Fig. 2A.

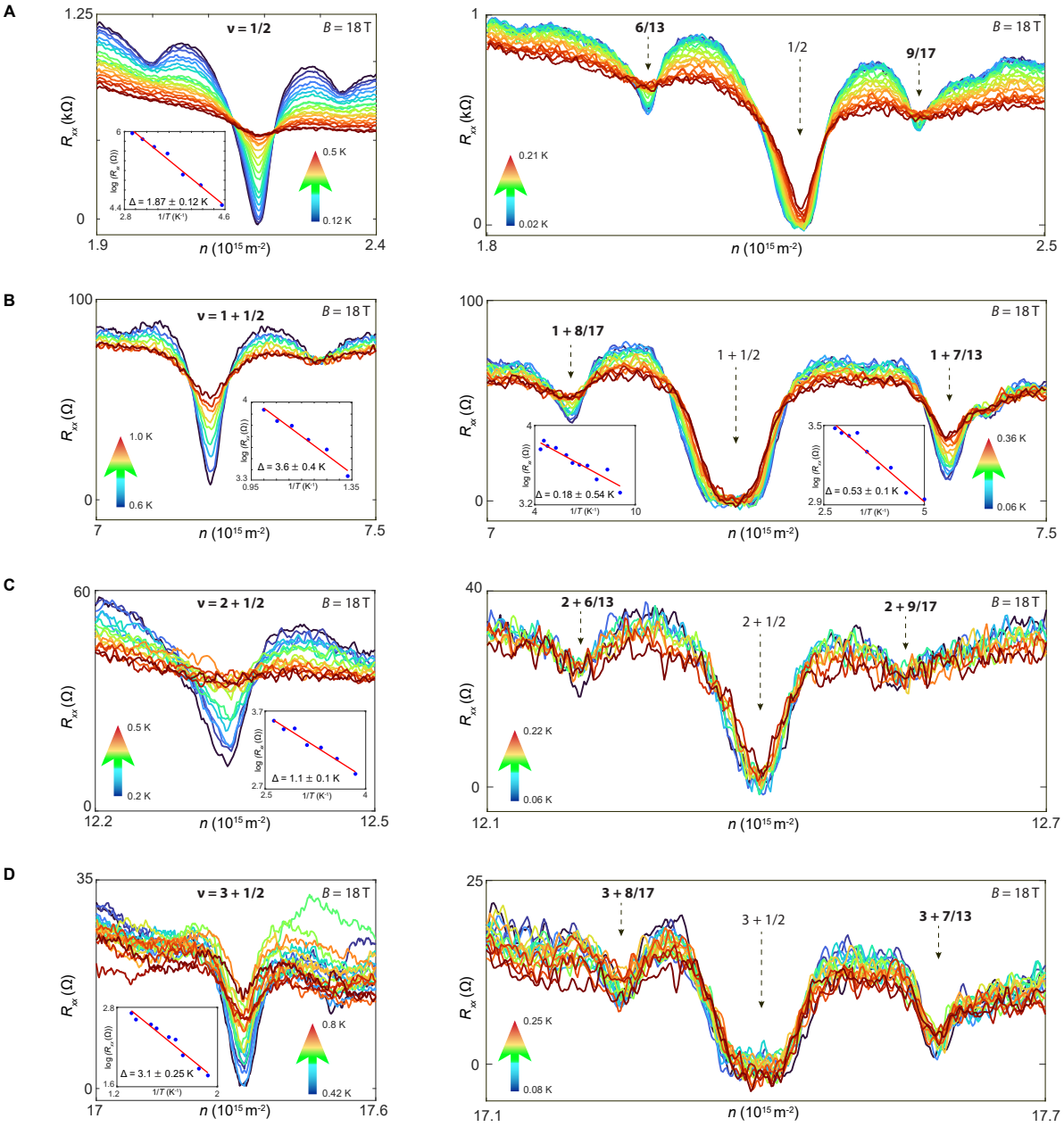


Supplementary Figure 7: R_{xx} as a function of ν and D from $\nu = 0$ to 4. Larger version of the electron side of Fig. 2A.

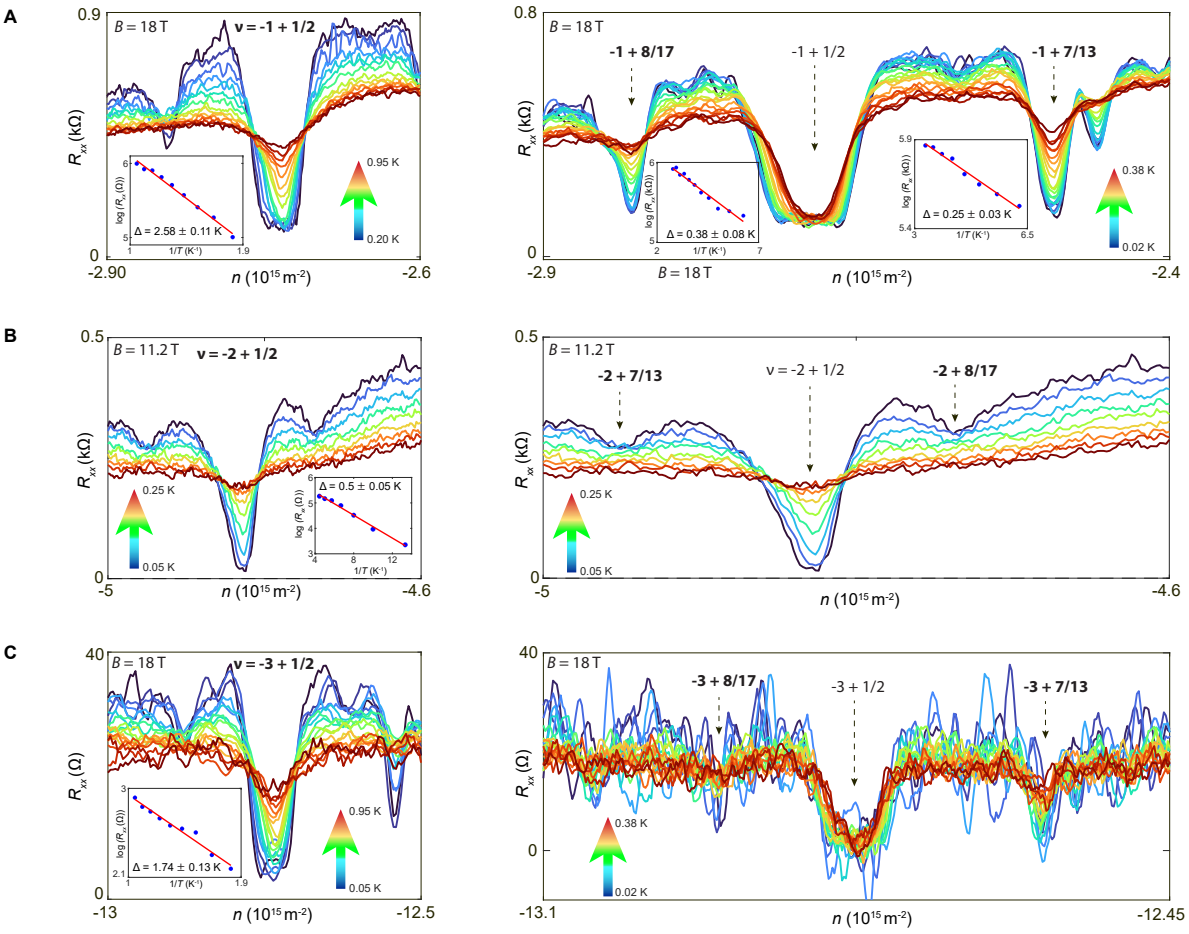
Section S5: Thermally activated transport measurements

Here (Figs. S8, S9, and S10), we present the experimental determination of the energy gap Δ of all the observed half- and quarter-filled states (except $\nu = -\frac{3}{2}$; see Sec. 10) along with their accompanying daughter states by temperature-activated measurements of R_{xx} at $B = 18$ T. We fit $\log R_{xx} \propto -\frac{\Delta}{2k_BT}$.

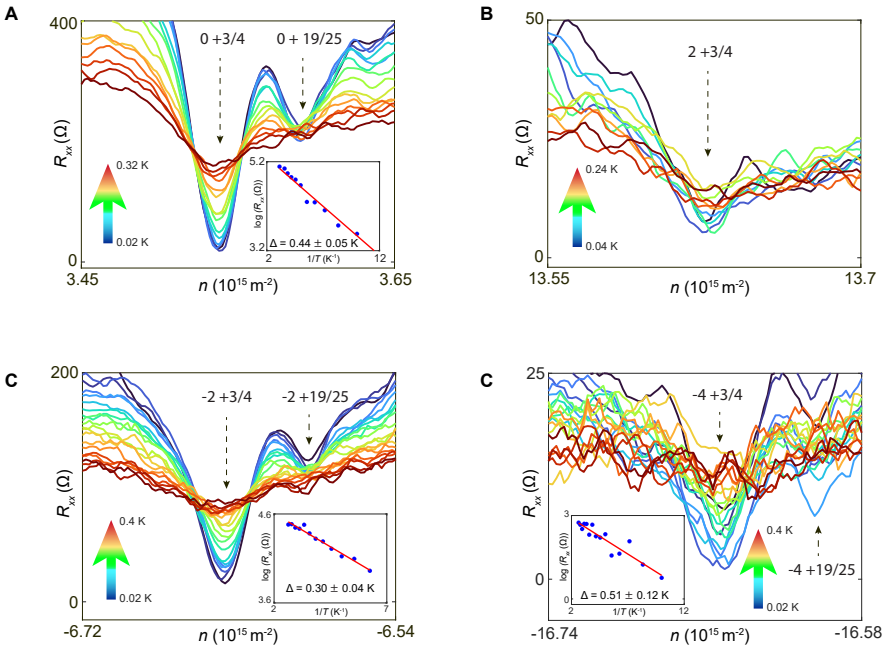
Left-hand panels in Figs. S8, S9, and S10 show R_{xx} versus n of the even-denominator states measured at different temperatures with fits shown in the insets. Right-hand panels show R_{xx} versus n of the even-denominator states, along with the accompanying daughter states measured at different temperatures. Notice that we use smaller temperatures for measuring the gap of the daughter states as they are much weaker compared to their parent states. For the weakest daughter states, we do not show linear fits but estimate an upper bound for the gap based on the temperature where there is no visible dip in the R_{xx} data.



Supplementary Figure 8: Activation gaps of all half-filled states (left panels) and their accompanying daughter states (right panels) observed on the electron side.

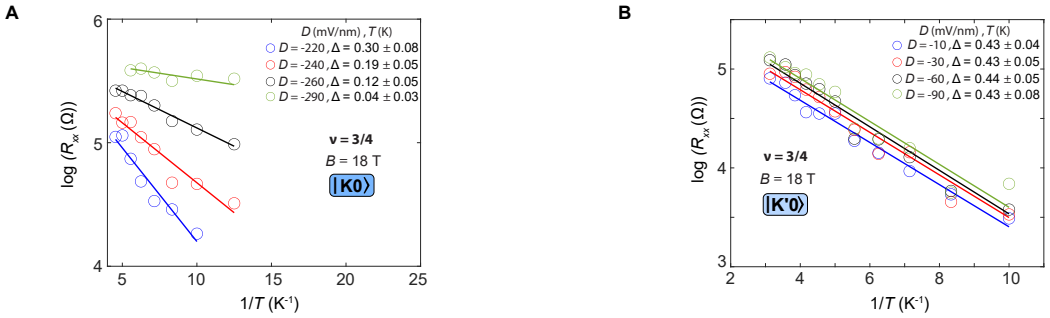


Supplementary Figure 9: Activation gaps of all half-filled states (left panels) and their accompanying daughter states (right panels) observed on the hole side.



Supplementary Figure 10: Activation gaps of all quarter-filled states.

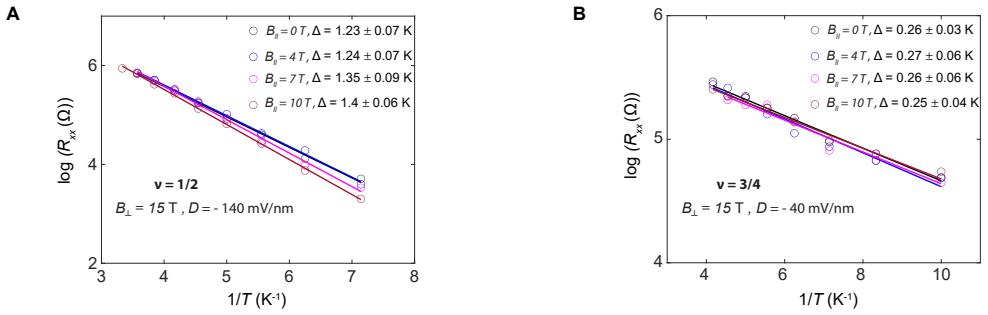
Section S6: Energy gap of $\nu = \frac{3}{4}$ in different valleys



Supplementary Figure 11: Activation gaps of $\nu = \frac{3}{4}$ measured in K (A) and $K^{'}$ (B) valleys at 18 T.

Section S7: In-plane magnetic-field measurements

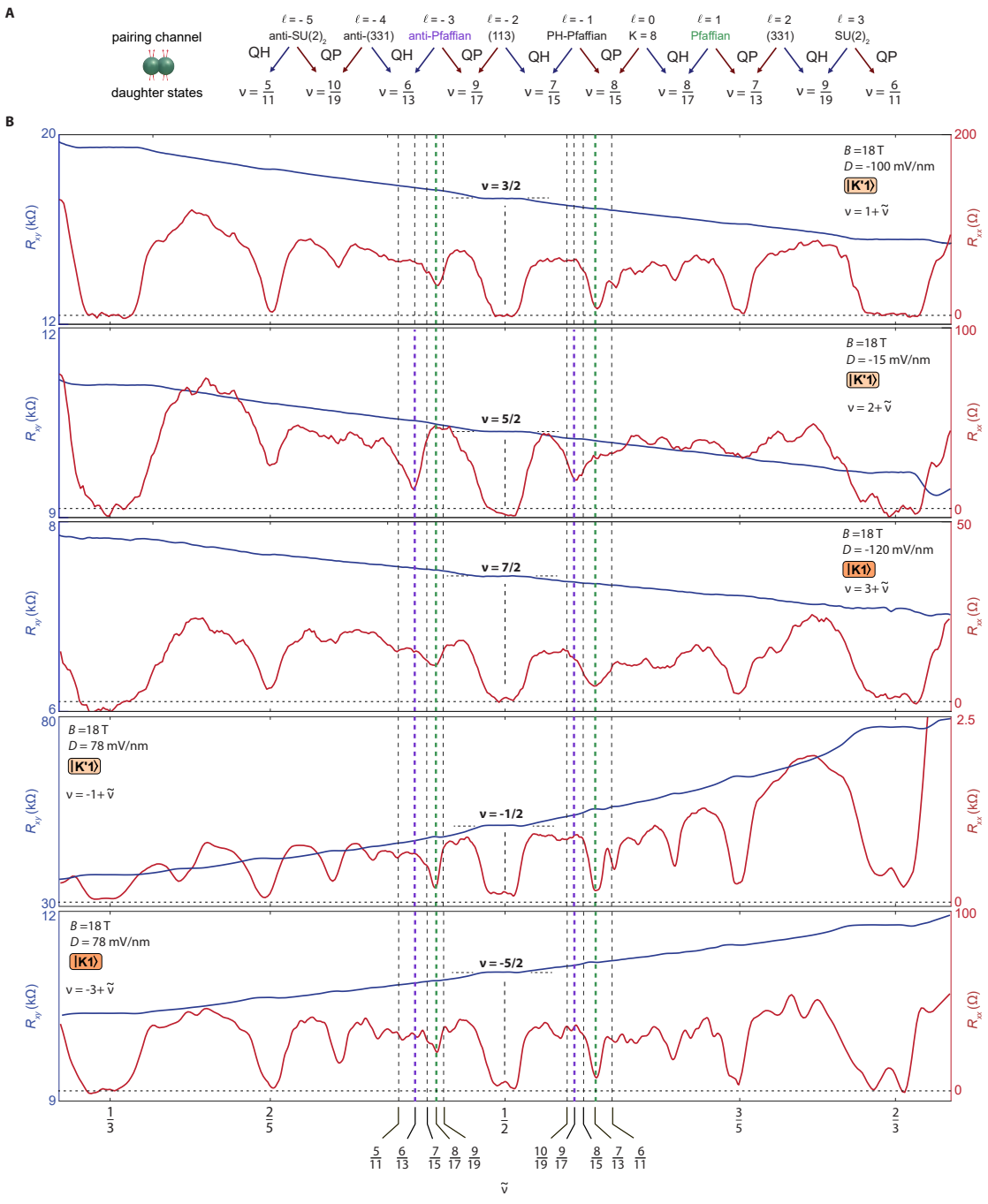
To determine the spin polarization of the newly observed $\nu = \frac{1}{2}$ and $\nu = \frac{3}{4}$ states, we rotate the sample at various angles inside the cryostat to achieve different in-plane magnetic field strengths (up to 10 T) such that the out-of-plane magnetic field remains constant at 15 T. Gaps for $\nu = \frac{1}{2}$ and $\nu = \frac{3}{4}$ at different in-plane fields are shown in Fig. S12.



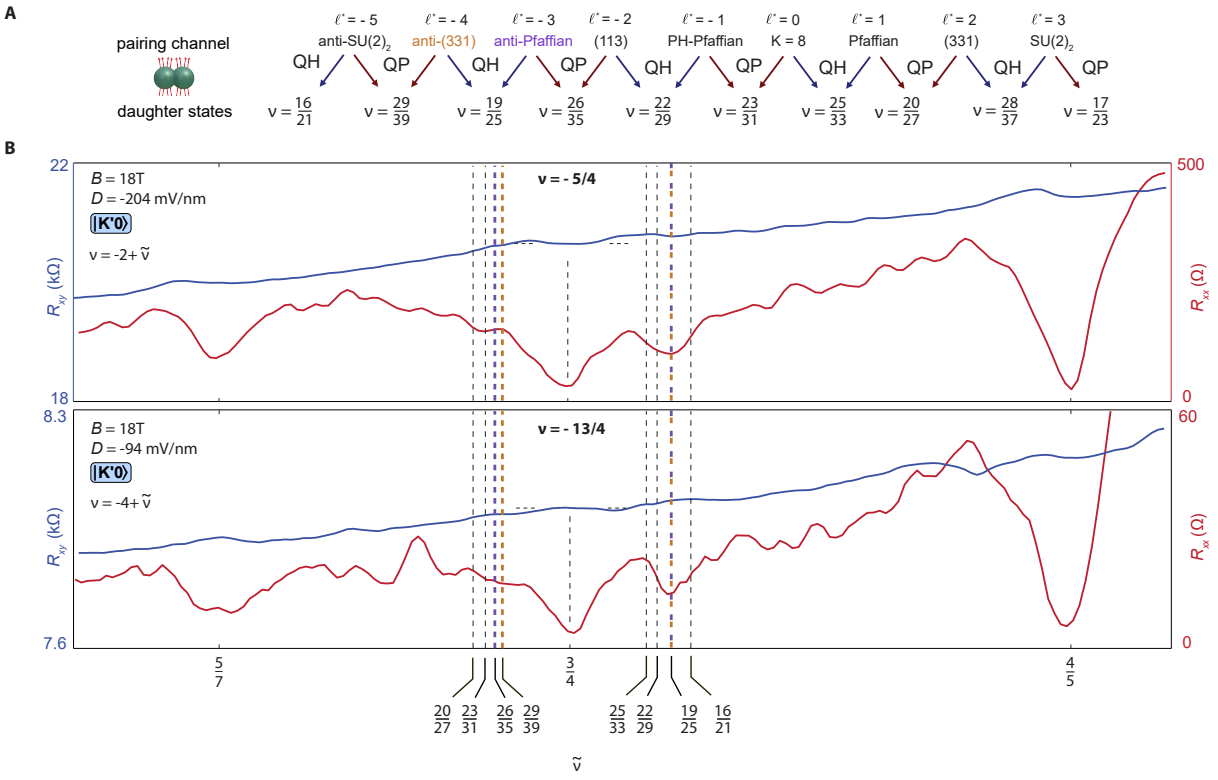
Supplementary Figure 12: Activation gaps of $\nu = \frac{1}{2}$ and $\nu = \frac{3}{4}$ measured as a function of the in-plane magnetic field at a constant perpendicular magnetic field of 15 T.

Section S8: All other half- and quarter-filled states and their daughters

Here in Fig. S13, we show line cuts of R_{xx} and R_{xy} from the D vs ν plots for different half-filled states, $\nu = \frac{3}{2}, \frac{5}{2}$, and $\frac{7}{2}$ on the electron-side and $\nu = -\frac{1}{2}$, and $-\frac{5}{2}$ on the hole-side. Vertical dashed lines mark daughter states fillings corresponding to the different pairing channels (shown in panel A). As mentioned in the manuscript, we identify the topological order (or pairing channel) in terms of $electrons$. The x-axis in Fig. S13 is defined as $\widetilde{\nu}$ which is positive for either sign of ν. The ν and $\widetilde{\nu}$ are related as $\nu = \widetilde{\nu} + [\nu]$. We use the same convention throughout the manuscript. In Fig. S13, $[\nu] = 1, 2, 3$ for $\nu = \frac{3}{2}, \frac{5}{2}, \frac{7}{2}$, and $[\nu] = -1, -3$ for $\nu = -\frac{1}{2}, -\frac{5}{2}$. In Fig. S14, we show quarter-filled states and their daughters at $\nu = -\frac{5}{4}$, and $\nu = -\frac{13}{4}$, where, $[\nu] = -2$ for $\nu = -\frac{5}{4}$, and $[\nu] = -4$ for $\nu = -\frac{13}{4}$.

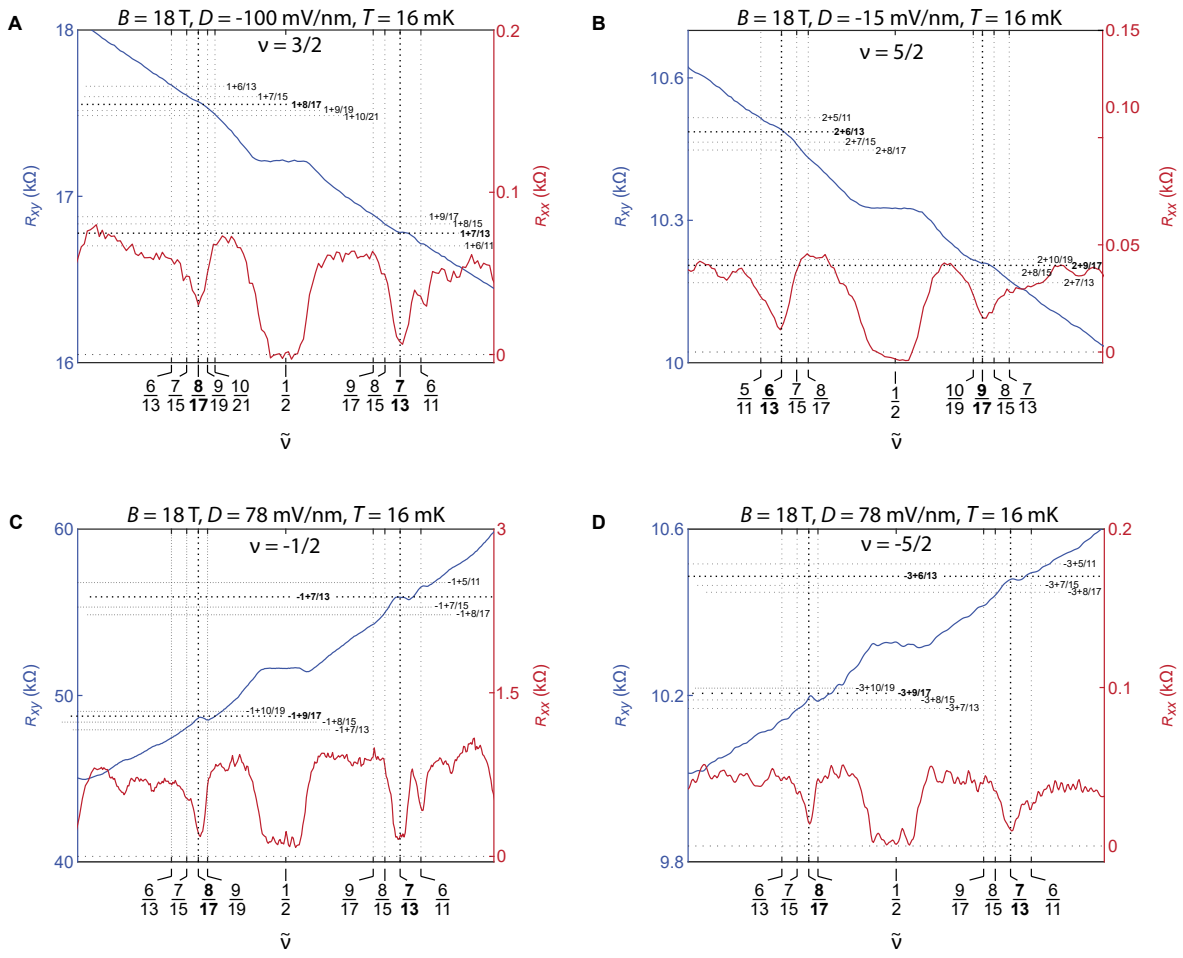


Supplementary Figure 13: Daughter states around $\nu = \frac{3}{2}, \frac{5}{2}, \frac{7}{2}, -\frac{1}{2}$, and $-\frac{5}{2}$.



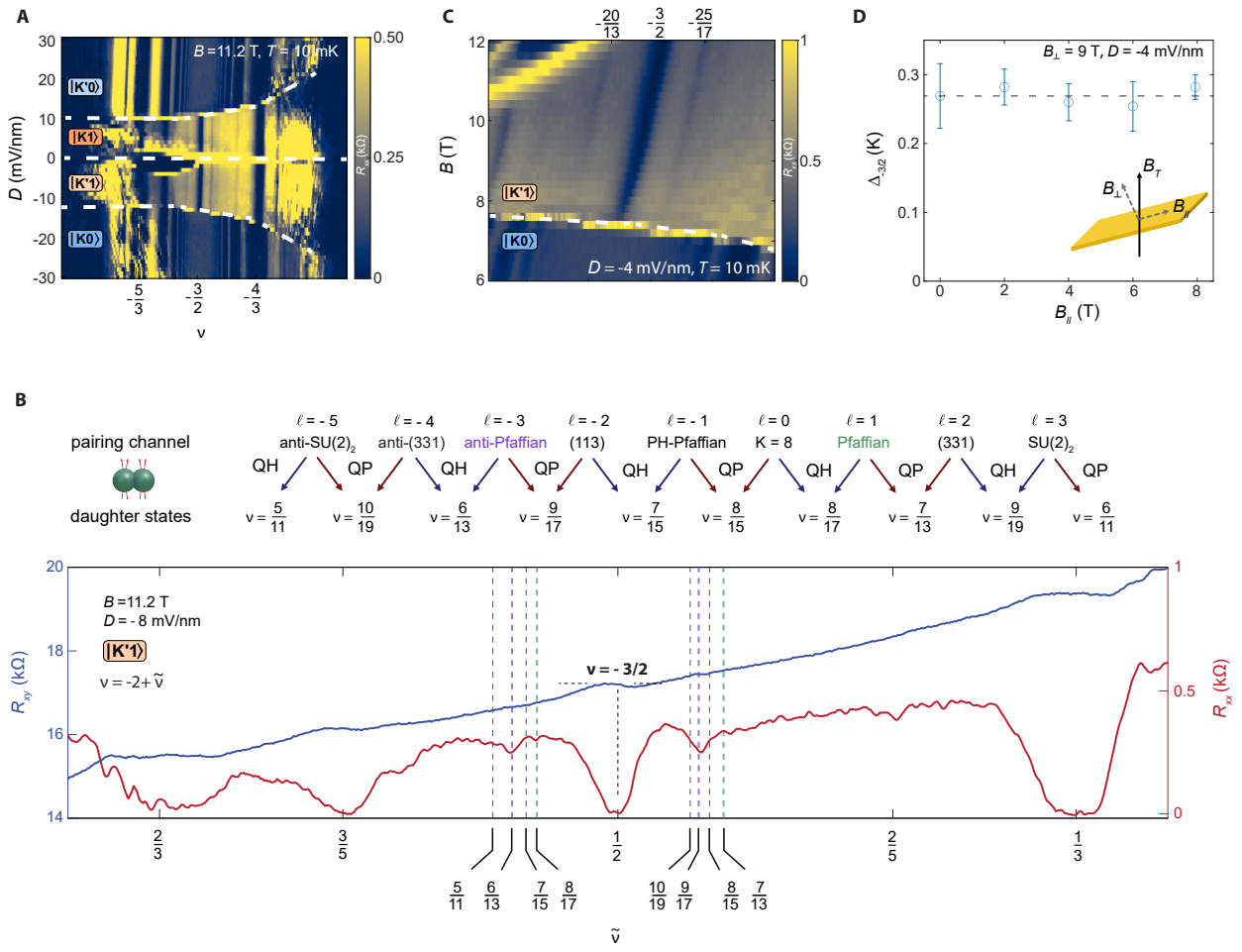
Supplementary Figure 14: Quarter-filled states around $\nu = -\frac{5}{4}$ and $-\frac{13}{4}$ and their daughters.

Section S9: Quantized plateaus at daughter-state fillings



Supplementary Figure 15: Quantized plateaus at daughter states. (**A**) Daughter states around $\nu = \frac{3}{2}$ showing good agreement with $\nu = 1 + \frac{8}{17}$ and $1 + \frac{7}{13}$, supporting a Pfaffian ground state. (**B**) Daughter states around $\nu = \frac{5}{2}$ showing good agreement with $\nu = 2 + \frac{6}{13}$ and $2 + \frac{9}{17}$, supporting an anti-Pfaffian ground state. (**C**) Daughter states around $\nu = -\frac{1}{2}$ showing good agreement with $\nu = -1 + \frac{8}{17}$ and $-1 + \frac{7}{13}$, supporting a Pfaffian ground state. (**D**) Daughter states around $\nu = -\frac{5}{2}$ showing good agreement with $\nu = -3 + \frac{8}{17}$ and $-3 + \frac{7}{13}$, supporting a Pfaffian ground state. All daughter states filling agree with the expected R_{xy} value.

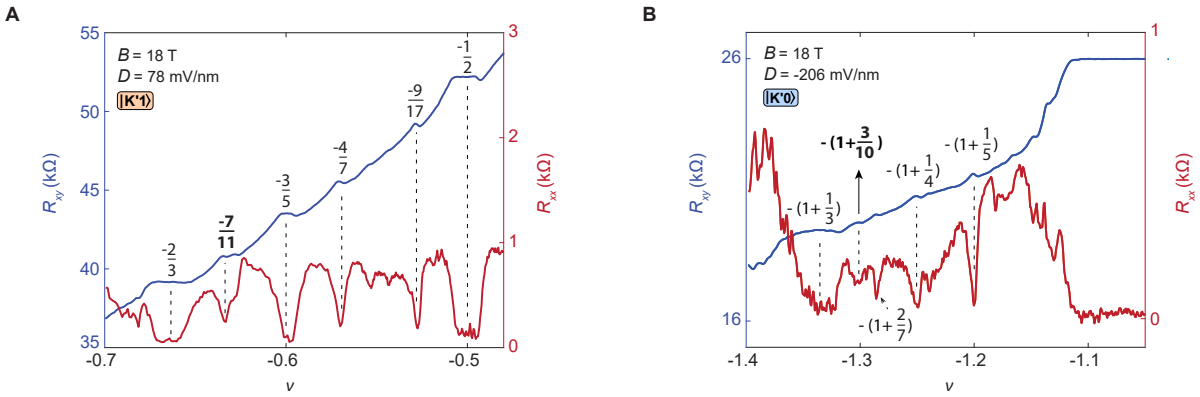
Section S10: Half-filled state at $\nu = -\frac{3}{2}$



Supplementary Figure 16: Characterization of $\nu = -\frac{3}{2}$. (**A**) R_{xx} as a function of ν and D at $B = 11.2$ T and $T = 10$ mK, clearly showing $\nu = -\frac{3}{2}$ flanked by daughters. (**B**) R_{xy} (blue) and R_{xx} (red) around $\nu = -\frac{3}{2}$ at $B = 11.2$ T and $D = -8$ mV/nm along with possible daughters marked by vertical dashed lines showing good agreement with an anti-Pfaffian ground state. (**C**) R_{xx} as a function of ν and B at $D = -4$ mV/nm and $T = 10$ mK. The state eventually disappears at the transition from $K'1 \to K0$. **(D)** The thermal activation gap $\Delta_{-\frac{3}{2}}$ as a function of $B_{\|}$ at $B_{\perp} = 9$ T and $D = -4$ mV/nm indicating that the state is fully spin-polarized.

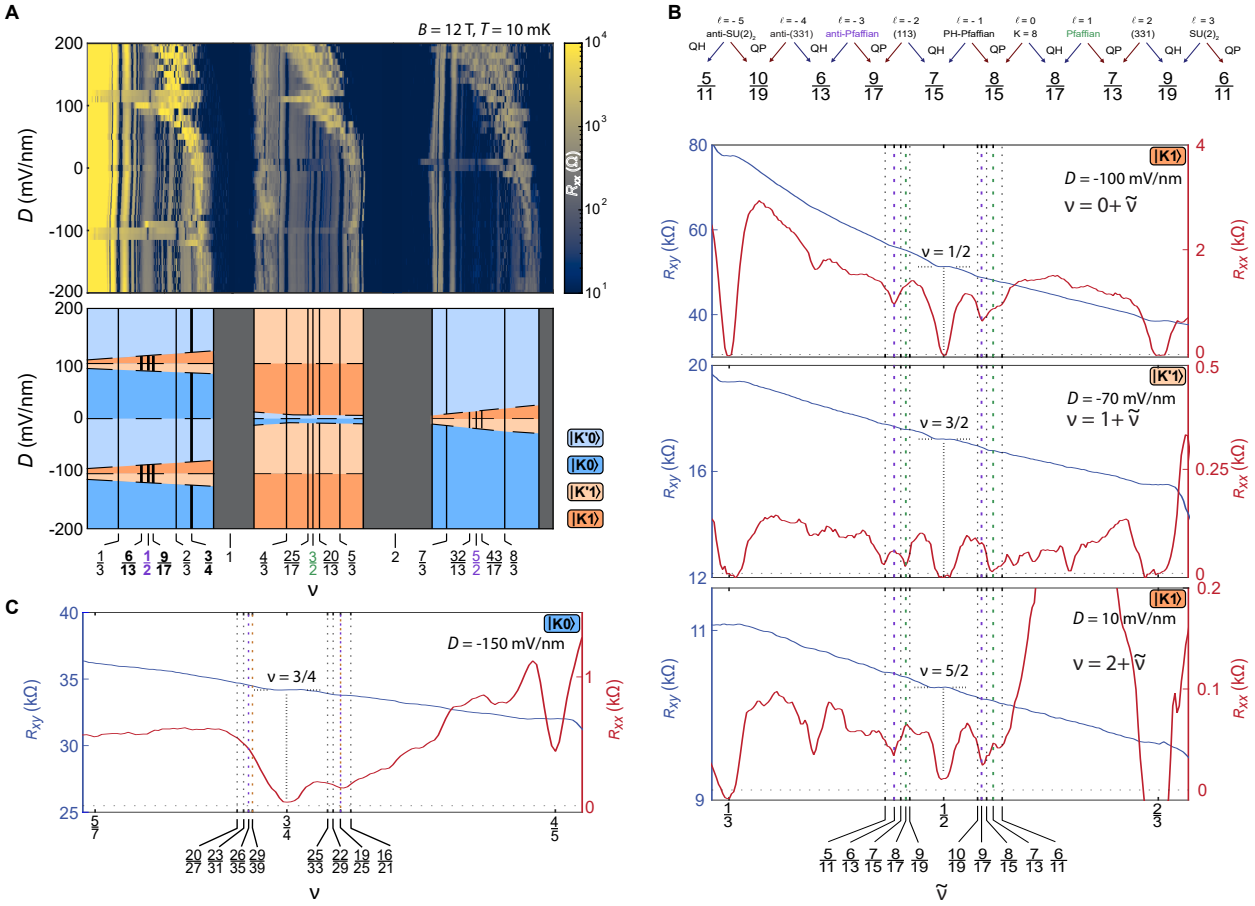
Section S11: Next-generation FQH states

Here we show FQH states observed at partial fillings of the LLs of ^{2}CFs.



Supplementary Figure 17: 'Next-generation' odd- and even-denominator FQH states at partially filled LLs of ^{2}CFs and ^{4}CFs. (**A**) R_{xy} (blue) and R_{xx} (red) versus ν measured on the hole side between $\nu = -\frac{1}{3}$ and $-\frac{1}{2}$. The filling $\nu = -\frac{7}{11}$ corresponds to $-\frac{7}{3}$ filling of ^{2}CFs LLs. (**B**) R_{xy} (blue) and R_{xx} (red) versus ν between $\nu = -1$ and $-(1 + \frac{1}{3})$. The partial filling $\nu = -\frac{3}{10}$ amounts to $-\frac{3}{2}$ filling of ^{4}CFs LLs.

Section S12: Data from device 2



Supplementary Figure 18: Data from device 2 measured at $B = 12$ T and $T = 10$ mK. (**A**) R_{xx} as a function of ν and D. The half-filled states $\nu = \frac{1}{2}, \frac{3}{2}$, and $\frac{5}{2}$ are clearly resolved. (**B**) Pairing channels (top) and R_{xx} and R_{xy} data around $\nu = \frac{1}{2}, \frac{3}{2}$, and $\frac{5}{2}$ showing the same daughters as device 1 (bottom panels). (**C**) R_{xx} and R_{xy} as a function of ν at $D = -150$ mV/nm, clearly showing a plateau at $\nu = \frac{3}{4}$ and a daughter state at $\frac{19}{25}$, the same as device 1.

Section S13: Paired composite-fermion states at $\nu = \frac{3}{4}$

Here, we discuss the possible paired composite-fermion states at $\nu = \frac{3}{4}$. The edge structures and thermal conductances of the most important candidates are shown in Fig. S16. They can be obtained in two ways: (i) In terms of ^{2}CFs, this filling factor corresponds to $\nu^* = -\frac{3}{2}$, which yields the required filling factor $\nu = \frac{\nu^*}{2\nu^*+1}$ of electrons. The composite fermions experience an effective magnetic field $B^* = -\frac{1}{2}B$, pointing in the opposite direction to the physical one. They fully occupy one ^{2}CF-Landau level (sometimes called Λ level) and half-fill the second one. The ^{2}CFs in the half-filled ^{2}CF-Landau level can form a paired quantum Hall state, analogous to electrons at half-filling of a physical Landau level. (ii) The filling $\nu = \frac{3}{4}$ is particle-hole conjugate to $\nu = \frac{1}{4}$. At the latter filling, ^{4}CFs are neutral and can form a paired superfluid. We show that the two approaches yield the same topological order.

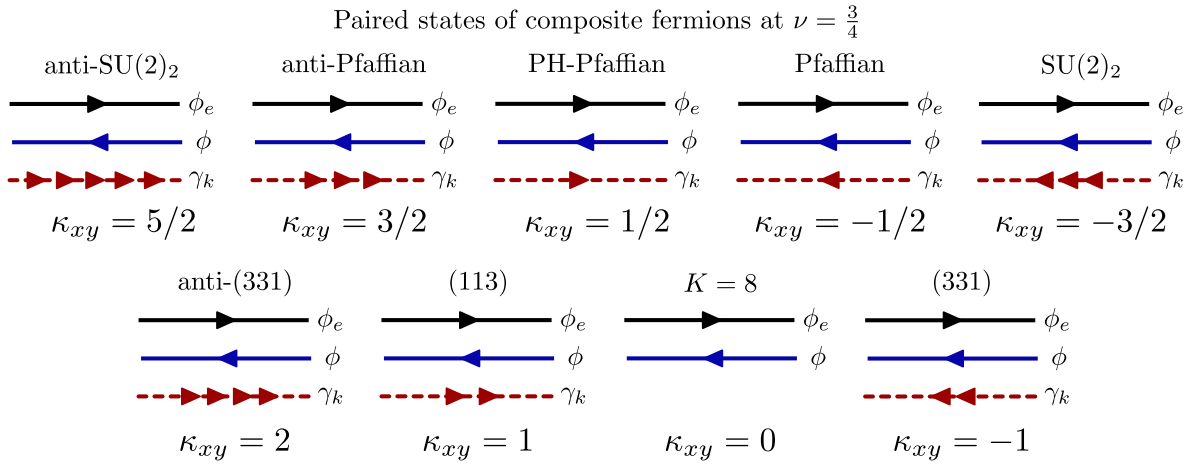
Two-flux CFs at $\nu^* = -\frac{3}{2}$: We first determine the edge structure of the ^{2}CF state at $\nu^* = -\frac{3}{2}$ and then infer the physical edge structure via flux attachment. The filled ^{2}CFs Landau level yields an integer edge mode (of composite fermions), and the half-filled level yields an additional semion mode. In the K-matrix description, these two edge modes are described by $K^*_{-3/2} = \mathrm{diag}(-1,-2)$ with $\mathbf{t} = (1,1)$. Both modes are propagating *downstream* with respect to the chirality dictated by B^*, which is *upstream* for B. In addition, depending on the pairing channel of the half-filled state, there are ℓ downstream (upstream) Majorana modes with respect to B^* (B). We are using this value ℓ when referring to the pairing channel of the $\nu = \frac{3}{4}$ state; see Fig. S16. The K matrix describing the physical edge of the $\nu = \frac{3}{4}$ is given by

$$K = K^*_{-3/2} + 2\mathbf{t}\mathbf{t}^T = \begin{pmatrix} 1 & 2 \\ 2 & 0 \end{pmatrix}. \tag{S1}$$

Its eigenvalues have opposite signs, implying that the two edge modes described by K move in the opposite directions. The direction of the Majorana modes is unaffected by flux attachment. The physical edge structure thus consists of two counter-propagating bosons and ℓ *upstream* Majoranas, resulting in the thermal conductance $\kappa = -\frac{\ell}{2}$. Recall that for electrons at $\nu = \frac{1}{2}$, the thermal Hall conductance is $\kappa = 1 + \frac{\ell}{2}$. In particular, the Moore–Read state at half filling has one *downstream* Majorana, while our naming convention assigns 'Moore–Read' at $\nu = \frac{3}{4}$ to a state with one *upstream* Majorana.

Particle-hole conjugates of paired ^{4}CF superfluids In the alternative approach, we first obtain $\nu = \frac{1}{4}$ states by pairing ^{4}CFs. Their edges are described by a single bosonic charge mode with $K_{1/4} = 4$ and ℓ *downstream* Majorana modes. Particle-hole conjugation [1,2] reverses the chirality of *all* modes and adds an integer electron mode that propagates oppositely to the $\nu = \frac{1}{4}$ charge mode. The physical edge is thus described by $K' = \mathrm{diag}(1,-4)$ and $\mathbf{t}' = (1,1)$ along with ℓ *upstream* Majorana modes. The thermal conductance along this edge is $\kappa = -\frac{\ell}{2}$, precisely as in Sec. 9.1. The K matrices we obtained in the two approaches are different. However, the $\mathrm{SL}(2,\mathbb{Z})$ transformation $W = \begin{pmatrix} 1 & 2 \\ 0 & -1 \end{pmatrix}$ shows that they encode

identical topological orders, i.e., $K' = W^T K W$ and $\mathbf{t}' = W^T \mathbf{t}$. Thus, we conclude that the two approaches result in the same phases of matter, the edge structures of which are depicted in Fig. S16 for the main pairing channels.



Supplementary Figure 19: The edge structures and thermal conductances of the most important $\nu = \frac{3}{4}$ candidates. States are identified by the pairing channel of ^{2}CFs, as explained in Sec. 9.1. The first row depicts non-Abelian states with an odd number ℓ of Majoranas; the second row shows Abelian states with an even ℓ.

References

1. Lee, S. S., Ryu, S., Nayak, C. & Fisher, M. P. A. Particle-Hole Symmetry and the $\nu = 5/2$ Quantum Hall state. *Phys. Rev. Lett.* **99**, 236807 (2007).

2. Levin, M., Halperin, B. I. & Rosenow, B. Particle-Hole Symmetry and the Pfaffian State. *Phys. Rev. Lett.* **99**, 236806 (2007).